STUDY OF THE EFFECT OF GRAIN STRUCTURE AND PHASE CONSTITUTION ON THE MAGNETIC PROPERTIES OF NANOCRYSTALLINE $Fe_{72.5}Cr_1Nb_3Cu_1Si_{13.5}B_9$ ALLOY

M. Sc. Thesis

BY

MD. TAHMID SHIHAB

DEPARTMENT OF PHYSICS

KHULNA UNIVERSITY OF ENGINEERING & TECHNOLOGY

KHULNA - 9203, BANGLADESH

MARCH - 2017

STUDY OF THE EFFECT OF GRAIN STRUCTURE AND PHASE CONSTITUTION ON THE MAGNETIC PROPERTIES OF NANOCRYSTALLINE $Fe_{72.5}Cr_1Nb_3Cu_1Si_{13.5}B_9$ ALLOY

BY

MD. TAHMID SHIHAB
ROLL NO: 1555553
SESSION: JULY - 2015

A THESIS SUBMITED TO THE DEPARTMENT OF PHYSICS, KHULNA UNIVERSITY OF ENGINEERING & TECHNOLOGY, KHULNA - 9203 IN PARTIAL FULFILMENT OF THE REQUIRMENT FOR THE DEGREE OF MASTER OF SCIENCE

DEPARTMENT OF PHYSICS
KHULNA UNIVERSITY OF ENGINEERING & TECHNOLOGY
KHULNA - 9203, BANGLADESH

MARCH - 2017

Dedicated

To

My Parents & Sisters

DECLARATION

This is to certify that the thesis work entitled as "**Study of the effect of Grain Structure and Phase Constitution on the Magnetic Properties of Nanocrystalline $Fe_{72.5}Cr_1Nb_3Cu_1Si_{13.5}B_9$ Alloy**" has been carried out in partial fulfillment of the requirement for M. Sc. degree in the department of Physics, Khulna University of Engineering & Technology, Khulna - 9203, Bangladesh. The above research work or any part of this work has not been submitted anywhere for the award of any degree or diploma. No other person's work has been used without due acknowledgement.

1. Supervisor

(Prof. Dr. S. S. Sikder)

Candidate

(Md. Tahmid Shihab)

2. Co-Supervisor

(Dr. M. A. Gafur)

Acknowledgements

I express all of my admiration and devotion to the almighty Allah, the most beneficial who has enabled me to perform this research work and to submit this thesis.

I wish to express my sincere appreciation and deepest sense of gratitude to my venerable teacher and supervisor Prof. Dr. Shibendra Shekher Sikder, Head, Department of Physics, Khulna University of Engineering & Technology (KUET), Khulna for suggesting the problem and for his affectionate guidance and inspiration during the course of this research work. He is always ready to provide a lucid explanation of the different concepts involved and critical reading of the script and subsequent corrections are much appreciated. Any mistakes that remain are of course mine. Without his constant supervision this thesis work could not performed.

I am very much indebted to my Co-supervisor Dr. M. A. Gafur, Principal Scientific Officer, PP & PDC, Bangladesh Council of Scientific and Industrial Research (BCSIR), Dhanmondi, Dhaka-1205, Bangladesh for his stimulating encouragement, sympathy, affection, guidance and valuable suggestion throughout the research work, who has consistent support and necessary motivation to progress my experimental works.

I am grateful to S. Manjura Haque, Head & Chief Scientific Officer, MSD, AECD, for providing kind opportunity to work in ther laboratory of Material Science Division for experimental work.

I am deeply grateful to Dr. Nazrul Islam Khan, PSO, MSD, AECD for his help in XRD analysis of the materials. I am grateful to Eng. F M Kamal S.E., Dr. Md. Mahbubul Haque S. S. O. of MSD, AECD for providing me with technical assistance from time during my research work at the laboratory of AECD.

I am indebted to Prof. Dr. Md. Mahbub Alam, Prof. Dr. Abdullah Elias Akhtar and Prof. Dr. Jolly Sultana, Department of Physics, KUET for their strong support in various ways the entire period of my study in this Department.

I am deeply grateful to Aninda Nafis Ahmed, Senior Engineer, Md. Rakibul Quadeer, Engineer and Sajib Aninda Dhar, Engineer, PP & PDC, Bangladesh Council of Scientific and Industrial Research (BCSIR), Dhanmondi, Dhaka-1205, Bangladesh, who helped me to understand annealing, XRD measurements and technical assistance in the laboratory and they were very much co-operative with me.

I am grateful to Mr. Md. Kamrul Hasan Reza, Associate Professor Department of Physics, KUET, Mr. Sujith Kumar Shil, Mr. Alamgir Hossain, Assistant Professor, Mr. Suman Halder , Mr. Suman Deb nath ,Lecture, Department of Physics, KUET for their tireless co-operation in my thesis work. I would also like to thank my well wishers and class fellows Robi and Tawhid.

I am also thankful to Ms. Alhamra Parvin, E.O., Ms. Anjummanara Begum J. E. O., Mr. Anawar Hossain S. S. A. Ms. Nazmunnahar Begum (S. A.-II), Ms. Jarna Begum (S. A.-II) of MSD, AECD, for their co-operation during the experiments and heartfelt help during the entire period of my research work at the laboratory of AECD. My thanks are due to the Director, AECD for his kind permission to use the laboratory of MSD, AECD.

A very special thanks to Mrs. Nandita Saha, spouse of Prof. Dr. S. S. Sikder for her heartfelt encouragement, cares and helps throughout the entire period of M. Sc. program.

I also wish to thanks the authority of Khulna University of Engineering & Technology (KUET), Khulna for providing me with the necessary permission and financial assistance for conducting this thesis work.

Md. Tahmid Shihab

ABSTRACT

This thesis is based on the experimental investigation of the effect of grain size and phase constitution on the magnetic properties of nanocrystalline $Fe_{72.5}Cr_1Nb_3Cu_1Si_{13.5}B_9$ alloys in the amorphous and annealed states. The sample has been prepared by rapid solidification technique and their amorphous nature has been confirmed by X-ray diffraction (XRD). The crystallization behavior and the nanocrystal formation have been studied by Differential Thermal Analysis (DTA) and XRD. Magnetization measurements have been carried out using vibrating sample magnetometer (VSM). The ribbon sample has been annealed in a controlled way in the temperature range 450^{o}C to 800^{o}C for 30 minutes. DTA runs for the sample show the existence of tow exothermic peaks one for $\alpha - Fe(Si)$ and other for Fe_2B phase. Thermal analysis experiment and from the obtained data activation energy of primary crystallization products $\alpha - Fe(Si)$ phase is 3.26eV and secondary crystallization products for Fe_2B is 4.87eV. The XRD experiments are in order to study the effect of structural parameters such as lattice parameter, grain size and silicon content of the nanocrystalline $\alpha - Fe(Si)$ grain. In the optimized annealing condition the grain size has been obtained in the range of 10-30nm. The peak shift indicates the change of the values of Si-content of nanograins and therefore, the change of the values of lattice parameter of nanograins. The saturation magnetization (M_s) has been observed 122.6emu/gm and in as prepared condition Curie temperature (T_c) has been found to be 316^{o}C, which quite close compared to the T_c of conventional FINEMET (i,e, sample without Cr). The critical composition for disappearance of ferromagnetism fall of curves M_s with the replacement Fe by Cr, where the nearest neighbor coupling to longer dominant and intermediate range occurs and the magnetization process of this amorphous ribbon sample are soft behavior of magnetic material.

Contents

CHAPTER III

EXPERIMENTAL DETAILS

CHAPTER IV

RESULTS AND DISCUSION

List of Figures

List of Tables

List of Symbols

a_0	=	Lattice parameter
B	=	Magnetic induction
D_g	=	Grain size
DTA	=	Differential Thermal Analysis
DSC	=	Differential Scanning Calorimetry
d	=	Average diameter
FWHM	=	Full Width at Half Maximum
H	=	Magnetic field
H_c	=	Coercivity
H_a	=	Applied magnetic field
[hkl]	=	Miller Indices
k	=	Magnetic hardness parameter
K_B	=	Boatman's constant
K_{eff}	=	Effective magnetic anisotropy constant
L	=	Self inductance of the sample core
L_o	=	Inductance of the winding coil without sample
L_{ex}	=	Ferromagnetic exchange length
M	=	Magnetization
M_s	=	Saturation magnetization
nm	=	nano meter
NM	=	Nobel metal
RAM	=	Random anisotropy model
RDF(r)	=	Radial Distribution Function
S	=	Total spin angular momentum
T_{ij}	=	Exchange interaction between atoms at the position r_i and r_j.
TTT	=	Temperature, time & transformation
T_a	=	Annealing temperature
T_c	=	Curie temperature
T_g	=	Glass transition temperature
T_x	=	Crystallization temperature
T_m	=	Melting point temperature

T_{x_1}	=	Primary crystallization temperature
T_{x_2}	=	Secondary crystallization temperature
T_{p_1}	=	Primary crystallization peak temperature
T_{p_2}	=	Secondary crystallization peak temperature
VSM	=	Vibrating Sample Magnetometer
XRD	=	X-ray diffraction
μ	=	Permeability
λ	=	Wave length
θ	=	Scattering angle
t_o	=	Time constant
β	=	Heating rate
δ_w	=	Domain wall Width
σ	=	Effective stress
$\rho(r)$	=	Atomic density
$< K >$	=	Average anisotropy
T_c^{am}	=	Curie temperature of residual amorphous matrix
ΔH	=	Enthalpy of crystallization
ΔE	=	Activation Energy

CHAPTER I

INTRODUCTION

CHAPTER II

THEORETICAL BACKGROUND

CHAPTER III

EXPERIMENTAL DETAILS

CHAPTER IV

RESULTS AND DISCUSSION

CHAPTER V

CONCLUSIONS

REFERENCES

INTRODUCTION

1.1 Introduction

The Present state of developments in the synthesis, structural characterization, properties and applications of nanocrystalline and amorphous magnets. More recently nanocrystalline materials have been investigated for applications in magnetic devices requiring magnetically soft materials such as transformers, inductive devices etc. Most recently research interest in nanocrystalline soft magnetic alloys has dramatically increased. The enhancement of soft magnetic properties requires reduction of crystalline grain sizes to a much smaller length scale that can overcome the anisotropy effects and result in an improved soft magnetic behavior. Nowadays, the attempts to understand different properties of materials on a smaller and smaller length scale are making footsteps for development of research in many area of material science. A new class of Fe-based alloys was introduced by Yoshizawa, Oguma and Yamauchi in 1988 which exhibited superior soft magnetic behavior. The material was produced by crystallization of an amorphous Fe-Si-B alloy with small addition of Cu and Nb. The identifying characteristic of the new material is its ultrafine microstructure of α-Fe(Si) phase/ DO_3 type with grain sizes of 10 – 15 nm from which their soft magnetic properties. These include coercivities of 0.01Oe and permeabilities of ~ 10^5. The alloy system, originally proposed as Fe-Cu-Nb-Si-B alloys, was manufactured by Hitachi Co. Ltd. under the trade names FINEMET [1.1]. With a view to improve the soft magnetic behavior of FINEMET type alloys, partial substitution of Fe with various elements has been widely investigated [1.2 – 1.3]. The FINEMET is cost effective and exhibit best soft magnetic properties. The FINEMET consists of a two phase microstructure in its optimally annealed condition. When these nanometric grains consolidate to form a nanostructural material, the magnetic properties are largely determined by the grain size and the exchange interaction between the adjacent grains [1.4]. Amorphous alloys provide an extremely convenient precursor material for the preparation of nanocrystals through the crystallization process controlled by thermal treatments [1.5 – 1.7]. These represent a new family of excellent soft magnetic core materials and have stimulated an enormous research activity due to their potential application [1.8 – 1.11]. The formation of this particular structure is attributed to the combined effect of Cu and Nb and their low solubility in bcc Fe. Cu is thought to promote the nucleation of Fe(Si) grain while Nb hinders their

growth and inhibits the formation of ferromagnetic Fe-B phases, which are contrary to soft magnetic properties, crystallization behavior and grain size are very much correlated with the magnetic properties. The soft magnetic properties of nanomaterials are connected with size, distribution of the nanometric grains, their composition, interfaces of constituent phases vanishing magnetic anisotropy, vanishing magnetostriction strong inter grain magnetic coupling and reduced magnetoelastic energy. The theoretical understands of the nanometric grain with magnetic softness has been consolidating in the light of Random Anisotropy Model proposed by Albens *et .al.* [1.12]. The magneto crystalline anisotropy of the small randomly oriented grains is averaged out of exchange interaction. To investigate the effect of Cu and Cr on the microstructural evolution from (Fe-Cr)-Si-B-Nb-Cu amorphous alloys to optimize the nanocrystalline microstructure for obtaining good soft magnetic properties in Cr containing FINEMET type alloys. In this work, the microstructural evolution by the crystallization $Fe_{72.5}Cr_1Nb_3Cu_1Si_{13.5}B_9$ melt spun amorphous ribbons will be investigated. To understand the mechanism of the formation of nanocrystals, size of the nanocrystals their volume fraction along with the effects on the magnetic properties through controlled thermal treatment will be studied.

1.2 The Aim and Objective of Present Work

The main objectives of the present work are to investigate $Fe_{73.5}Cr_1Nb_3Si_{13.5}B_9$ nanocrystalline ribbon and to study the phase constitution and magnetic properties.
The objectives of the research work are as follows:

- To synthesize the $Fe_{72.5}Cr_1Nb_3Cu_1Si_{13.5}B_9$ alloy in the form of ribbon in the amorphous state by rapid solidification technique.
- To study growth of nanocrystals on amorphous matrix by thermal treatment.
- The formation nanocrystals with grain size distribution as affected by heat treatment with varying temperature and holding time.
- The nanoensembles and their bulk magnetic properties will be studied.
- Correlation of the evaluations of nanograins with the magnetic properties.
- Find out the optimum composition and grain distribution affecting the magnetic properties of this system.

1.3 Experimental Reason for Choosing this Research Works

In the present work, soft magnetic amorphous FINEMET type alloy nominal amorphous ribbon with composition $Fe_{72.5}Cr_1Nb_3Cu_1Si_{13.5}B_9$ will be prepared for high purity ingredients by rapid solidification technique using a melt spinning machine. To improve the magnetic properties of this amorphous ribbon microstructure is an important parameter that can be controlled by heat treatment condition.

The experimental methods that would be used in this research work are as follows:

- Amorphousity of the samples will be checked by X-ray diffraction.
- Differential thermal analysis (DTA) will be used to evaluate the phase transformation and to determine the crystallization temperature. From the DTA analysis evaluation of the crystallization activation energy of various phases will be done.
- The optimum heat treatment would be carried out in a microprocessor controlled high temperature furnace.
- Crystallization phase and grain size of the nanograins will be determined by XRD on samples annealed at different temperatures.
- Magnetization of the samples will be measured as a function of magnetic field and temperature using a vibrating sample magnetometer (VSM).

Optimum annealing temperature would be ascertained through isothermal annealing over a wide range of temperature. An estimation of the volume fraction of the nanocrystalline Fe-Si phase has been ascertained from the thermo magnetic measurement depending on the annealing temperature. It is expected that the use of grain size affected heat treated sample may give uniform microstructure exhibiting better magnetic properties. The low percent of Cr-substituted Fe-based nanocrystalline alloy provided the volume fractions of crystallites are very low. If the grain size of the nanocrystal is small enough and the intergranular amorphous matrix is sufficiently thick to minimize the magnetic interactions between them, the super paramagnetic behavior of the nanocrystalline particle is expected.

1.4 Application of Nanocrystalline Ribbons

Early discoveries of magnetic amorphous metallic glasses, their promise for soft magnetic applications has continued to be exploited. Soft magnetic ribbons produced by rapid quenching from the melt are already used in the industrial uses

practices. Magnetic properties of specific composition greatly profit from the thermal treatment that leads to partial crystallization where nanoscale crystalline grain are embedded in the amorphous of the alloy. Recently, however, a revolution in the understanding of magnetic properties on a nanoscale and the discovery of exciting new nanocrystalline magnetic materials has led to be vital for application of these soft magnetic materials. It appears that a significant need for state of the art application of soft magnetic materials will include high temperature performance of soft magnetic materials.

Nanocrystallization of amorphous precursors has also required compaction to produce shapes and to improve mechanical properties as ribbon is quite brittle after nanocrystallization. Fe based nanocrystalline ribbons can be used to replace silicon steel, permalloy and ferrites. These are excellent materials to make transformers core for high frequency switch mode power supplies, current transformer cores, transformer cores for ground –fault-interrupters, cores for filters, storage inductors, and reactors, EMC common modes chokes ,sensor cores, cores for saturable reactors, magnetic amplifiers, beads ,and pulse compressors.

Operation of the IPU at the high temperatures associated with air cooling requires materials with excellent high temperature magnetic and mechanical properties. Realization of these exciting potentials will require:

(i) Development of high permeability, large saturation and remnant induction, low loss, hysteresis and eddy current for soft magnets of operating at high temperature.

(ii) Development of high energy product permanent magnets capable at operating at high temperatures.

(iii) Improved mechanical properties and corrosion resistance at higher operating temperatures.

(iv) Development of new magnetic device geometrics which exploit the materials.

Nanocrystalline materials have no microstructural discontinuities such as dislocations, grain boundaries or precipitates. This significantly reduces the possible spinning sites for domain walls, reducing the coactivity.

1.5 Review of Research on FINEMET

It has been well established by the time through extensive research work that the addition of Cu and Nb simultaneously with Fe-Si-B based amorphous alloys is the necessary condition for the extraordinary soft magnetic properties of the FINEMET alloy. This addition extends the temperature range between the primary crystallization α-Fe(Si) temperatures T_{x1} and secondary crystallization Fe-B temperature, Tx_2 premiere for achieving superior magnetic properties [1.13]. It should be stressed again that good soft magnetic properties require not only a small grain size but at the same time the absence of boron compounds.

The formation of typical nanocrystalline structure is given by a primary crystallization process before the stable or meta-stable inter atomic phases are formed obviously this can be attained by (i) alloying additions which lead clearly separated stages of crystallization at T_{x1}andT_{x2} and (ii) by annealing at $T_{x_1} < T_a < T_{x_2}$ such that only the phase forming at and above T_{x1} is crystallizing. Murillo *et. al.* [1.14] studied the influence of Cu/Nb content and annealing conditions on the microstructure and the magnetic properties of FINEMET alloys. Grain size, phase composition and transition temperatures were observed to depend on the ratio of Cu/Nb content. Amorphous ferromagnetic material based on Fe-Si-B show good magnetic properties when they are heat treated below their crystallization temperature while the Fe-Cu-Nb-Si-B alloys exhibit extraordinary high permeability, two orders of magnitude higher than their conventional Fe-Si-B alloys due to heat treatment just above the crystallization temperature for a specific time. The great scope of technical application this material $Fe_{73.5}Nb_3Cu_1Si_{13.5}B_9$ arise from this freedom of tailoring the magnetic properties [1.15-1.18].

The study of Yoshizawa *et al.* [1.19] and Noh *et al.* [1.20] on the role of nucleating agent Cu on the crystallization behavior of the composition $Fe_{73.5}Nb_3Cu_1Si_{13.5}B_9$ revealed that the average grain size is relatively large at crystallization temperature due to lower crystallization rate with no addition of Cu and annealing of this Cu free alloy leads to simultaneous or sequential formation of several crystalline phases. Kataoka *et al.* [1.21] verified the role of Au in place of Cu and reported the Au is the only element, which has a comparable effect on the crystallization behavior. They also found that the average grain size just after the onset of crystallization is relatively large up to about 60nm with a broad scatter and

show a distinct variation with the annealing temperature. This indicates the significantly lower nucleation rate than in the Cu-doped alloy whose finer grain size is almost constant in a wide range of annealing temperature [1.22].

Inoue *et al.* [1.23] observed that group IVa and VIa transition metals extends the glass forming range at low Si or B contents. The glass forming range is the widest for Hf containing alloys and decreases in the order. According to Suzuki *et al.* [1.24-1.25] the glass forming ability is considerably improved with the addition of Hf or Zr.

Herzer [1.26] studied on Curie temperature and permeability of nanocrystalline material. According to him when measuring temperature approaches the Curie point of the inter-granular amorphous phase, the exchange coupling between the crystallites is largely reduced. As a result, the initial permeability drops down. As reported by Hakim *et al.* [1.27] and S. Manjura Haque *et al.*[1.28], magnetic initial permeability of nanocrystalline amorphous ribbon strongly depends on annealing temperature and exhibits super paramagnetic behavior at $T > T_c^{am}$. When T_c^{am}, the grain coupling is largely but not interrupted above T_c^{am} and still persists to higher value of permeability compared to annealed temperature at T_c^{am} exhibiting the magnetic coupling between particles is significant. The precise coupling mechanism for this type of behavior at $T > T_c^{am}$ may be explained in terms of exchange penetration through thin paramagnetic inter-granular layer and/or dipolar interactions.

Franco *et al.* [1.29] also studied the super paramagnetic relaxation in FINEMET type of alloy Fe-Cu-Nb-Si-B without adding any extra refractory element and they have demonstrated that, this behavior is a general characteristics of this nanocrystalline alloys provided the volume fraction of crystallites are very low. If the size of the nanocrystals is small enough and the inter-granular amorphous matrix is sufficiently thick to minimize the magnetic interactions between them, of the nanocrystalline particles is expected.

Magnetic and structural properties of FINEMET alloy and with the substitution of Nb by Ta, Mo and Cr, W have been studied by several investigators [1.30-1.31]. Results show that FINEMET composition with Nb an Ta show similar soft magnetic characteristics while alloy with substitution of Nb and Cr, Mo and W display somewhat lower soft magnetic properties. Hakim *et al.* [1.32] found with the Ta substituted alloy super paramagnetic and super ferromagnetic behavior depending upon the volume fraction of the nanocrystallites from the temperature dependence of permeability of the samples annealed in the temperature range 500 - 575^{o}C. Similar

behavior of super paramagnetic has been observed in the FINEMET alloy with higher content of Cr substituted for Fe [1.33-1.34]. Magnetic properties of partial substitution of Fe by Cr have been studied by several investigators with a limited concentration of Cr between 1 and 5 at. % substituted for Fe in the FINEMET alloy [1.35-1.37]. The authors found that Cr enhances the crystallization temperature, controls the volume fraction and particle size of α-Fe(Si) phase and reduces the Curie temperature. The influence of Cr content with higher percentage of Cr on the magnetization behavior of $Fe_{73.5-x}Cr_xNb_3Cu_1Si_{13.5}B_9$ alloys have been studied [1.38]. It has been found that magnetic moment and the T_c decreases linearly with Cr concentration. The onset of ferromagnetism for the alloy system studied has been claimed to be Cr < 27 at. % and the alloys have been found to follow the Bloch's $T^{3/2}$ - law in their temperature dependence of magnetization.

The effect of annealing temperature on saturation magnetization (M_s) has been reported by Lovas *et al.* [1.39] and Berkowitz [1.40]. M_s is increased with annealing temperature up to initial stage of crystallization temperature and then decreases correspond to the optimum nanocrystallized state with high volume fraction of Fe (Si) nanograins. The influence of low concentration of Cr on the magnetization, structural behavior of $Fe_{72.5}Cr_1Nb_3Cu_1Si_{13.5}B_9$ alloy has been studied.

1.6 Organization of the Thesis

The thesis has been divided into five chapters.

Chapter-I general introduction followed by The aim and objectives of the present work, reason for choosing this research work, application of nanocrystalline ribbons, review of researches on FINEMET and organization of the thesis.

In Chapter-II, the theoretical background of the stability of amorphous alloys, theories of magnetization are discussed.

In Chapter-III, the preparation procedures of the nanocrystalline alloys are described, the experimental details including Differential Thermal Analysis (DTA), X-ray Diffraction (XRD) analysis, and Vibrating Sample Magnetometer (VSM) are described.

In Chapter IV, the details results regarding DTA, activation energy, corresponding crystallization temperature, XRD method after heat treatment of the sample at different temperatures, Lattice parameter, Silicon content, Grain size

determination, field dependence of specific magnetization and annealing effects on saturation specific magnetization are discussed.

And Chapter V contains conclusion, achievement of works and further suggestion of this work.

Finally a complete list of reference has been given towards the end of the chapters.

THEORETICAL BACKGROUND

2.1 History of Nanocrystalline Materials

A new class of Fe-based alloys was introduced by Yoshizawa, Oguma and Yamauchi, in 1988 which exhibited superior soft magnetic behavior. The material was produced by crystallization of an amorphous Fe-Si-B alloy with small additions of Cu and Nb. The identifying characteristic of the new material is its ultrafine microstructure of Fe(Si) with grain sizes of 10-15nm from which their soft magnetic properties emerge. These include coercivities of 0.01Oe and permeabilities of ~ 10^5. The alloy system, originally proposed as Fe-Cu-Nb-Si-B alloys, was manufactured by Hitachi CO. Ltd. Under the trade names FINEMET [2.1]. The originally proposed composition was $Fe_{73.5}Cu_1Nb_3Si_{13.5}B_9$. The unique properties of FINEMET alloys include low losses, high permeability and near zero magnetostriction achieved by permelloy and Co-based amorphous alloys, but much higher saturation magnetization up to 1.3 Tesla, than these materials usually have ever offered.

From the nanometer regime to macroscopic grain sizes, the permeability shows an analogous behavior being essentially inversely proportional to H_c. Coercive force is thought to be inversely proportional to D_g. Lowest coercivities, however are again found for smallest structural correlation lengths like in amorphous alloys and in nanocrystalline alloys for grain sizes < 20nm. Therefore, main efforts to improve the soft magnetic properties are directed to make the crystal grain size larger and / or to make the magnetic domain size smaller by annealing and working.

According magnetic softening should occur as soon as the structural correlation length or D_g becomes smaller than the E_{ex} which is in the order of domain wall width. In this case, the local anisotropies are randomly averaged out by exchange interaction so that there is no anisotropy net effect on the magnetization process. It is well accepted that good magnetic properties are obtained when $D_g << L_{ex}$ [2.2]. However, FINEMET demonstrated a new phenomenon; reduction of grain size, "to a nanometer level", improves the soft magnetic properties significantly. In this nano-world, the H_c is directly proportional to D_g, D_g on the order of D_g^2 to D_g^6.

2.1.1 Composition of the Nanocrystalline

The study of magnetic glass dates back to the pioneering work of pol. Duwez at Caltech in the 1950s. Duez employed atomization [2.3] prior to splat quenching [2.4-2.6]. Ferromagnetic amorphous alloy were first reported by Mader and Nowik [2.7]. Soon after, Tsuei and Duwez [2.8] reported splat quenched amorphous ferromagnetic with interesting soft magnetic properties.

Generally the optimum mechanical and magnetic properties of nanocrystalline soft magnetic materials are obtained for partially crystallized materials. This means that those materials are formed in two phases [2.9]. In general nanocrystalline alloys can be described as TL_{1-x} (TE, M, NM)$_x$ where

- TL denotes a late ferromagnetic transition metal element (TL= Co, Ni or Fe)
- TE denotes an early transition metal element (TE = Zr, Nb, Hf,Ta etc.)
- M is metalloid (M = B, P, Si, etc.) and
- NM is a noble metal (NM=Cu, Ag, Au etc.)

This composition usually has $x < 0.02$ i.e. with as much late ferromagnetic transition metal (TL of Fe, Co or Ni) as possible. The remaining early transition metals (TE = Zr, Nb, Hf, Ta, etc.) and metalloids (B, P, Si, etc.) are added to promote glass formation in the precursor. The noble metal elements (NM = Cu, Ag, Au, etc.) serve as nucleating agents for the ferromagnetic nanocrystalline phase. The compositions are limited by where glass formation can occur prior to the nanocrystallization route. These alloys may be single phase (Type-I) but are generally two phase materials with a nanocrystalline ferromagnetic phase and a residual amorphous phase at the grain boundaries (Type-II).The type-II nanocrystalline alloys might have general properties:

- Relatively high resistivity (50 - 80μΩ-cm)
- Low magnetocrystalline anisotropy and
- Increase mechanical strength

With properties such as these, nanocrystalline alloys have great potential as soft magnetic properties. In the ongoing research we are any interested about the type-II.

Nanocrystalline soft magnetic alloys have received considerable attention due to their excellent soft magnetic properties [2.10]. Small addition of Cu and Nb into Fe-Si-B amorphous materials charges considerable their crystallization process, which

is executed under appropriately controlled conditions and the specific purpose of these addition are

- The element is used for helping the formation of nuclei and ultra-fine grain and
- The element is used to impede the growth of the crystallites.

In this material, the nanocrystalline state is composed of a fine structure of α-Fe (Si) and is usually around 10nm. For such as average grain size the exchange interaction dominates the magnetic behavior of randomly oriented crystallites guided by random anisotropy [2.11]. In the present thesis work nanocrystalline alloy is prepared by one percent substitution of Fe by Cr of FINEMET $Fe_{73.5}\,Nb_3\,Cu_1\,Si_{13.5}\,B_9$.

2.1.2 An overview of Nanocrystalline Materials

Nanocrystalline amorphous ribbon can be considered as an off-shoot of 1amorphous materials. In fact nanocrystalline amorphous ribbon is a composite material where nanocrystals are embedded in an amorphous matrix. Nanocrystalline materials represent one of the most active research areas in recent times for the atomic tailoring of materials with specific properties and property combinations. In addition to the understanding of the usual properties possessed by nanophase materials, there are three other associated areas, which need serious attention:

(i) Identification and development of suitable preparation methods, especially those which are capable of providing large industrial quantities of nanometer scale materials.

(ii) Development of processing methods for manufacturing these materials into useful size and shapes without losing their desirable nanometer size feature and

(iii) Identification of proper characterization methods, where the nanometer size range of these materials falls just below or at the resolution limit of the conventional tools.

2.2 Alloy Design Issues

Alloy design issues include issues of chemistry and processing designed to:

(i) Optimize one of a number of important intrinsic and or extrinsic magnetic properties and

(ii) Optimize structural or microstructural features which promote important magnetic properties.

The first of these issues concerns the choice of chemistry so as to impact the intrinsic magnetization of the material. The second issue pertinent to alloy additions designed at aiding formation of an amorphous phase.

Since microstructure of alloy in influence extrinsic magnetic properties, the important microstructure features should be recognized including grain size, shape and orientation, defect concentration, compositional in homogeneities, magnetic domain and domain wall. The development of soft magnetic materials for application requires attention to a variety of intrinsic magnetic properties as well as development extrinsic magnetic properties though an appropriate optimization of the microstructure.

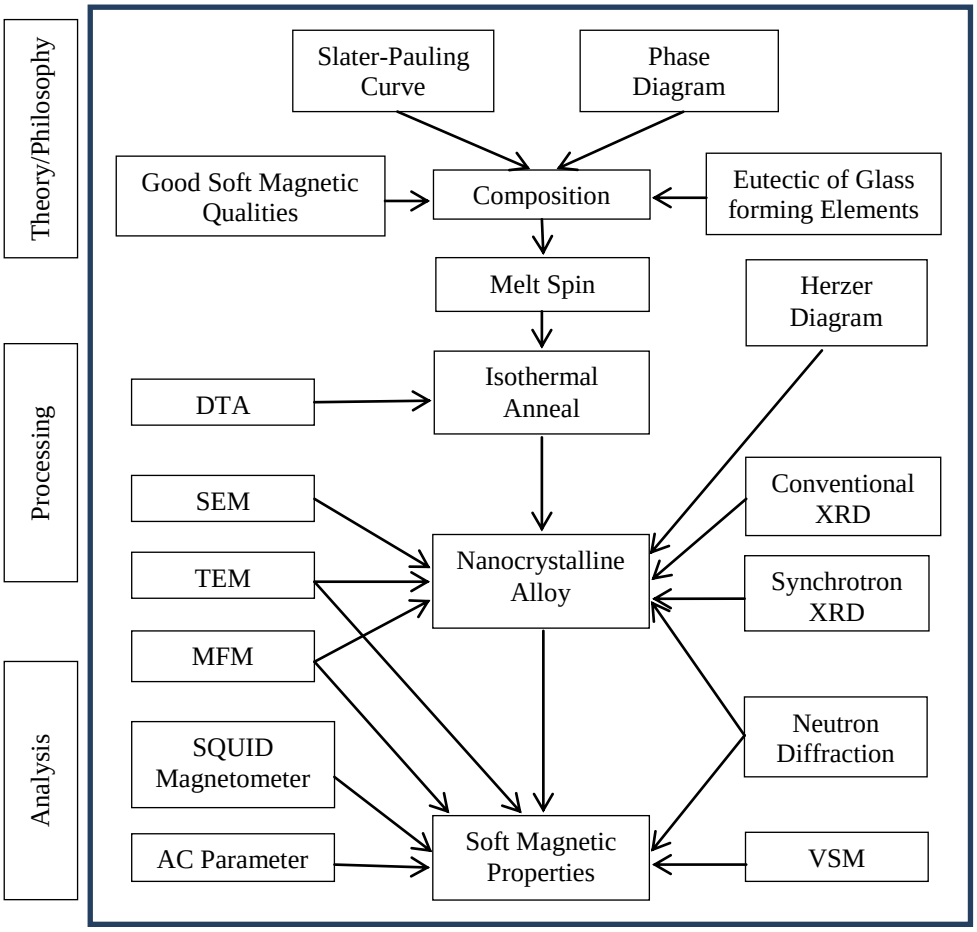

Figure 2.1 Flowchart for the consideration in designing and developing nanocrystalline soft magnetic material from an amorphous precursor route

Alloy design issue are in many was influenced by processing routes used to achieve desired microstructures. In Figure 2.1 illustrates a flowchart for the considerations in designing and developing nanocrystalline soft magnetic material from an amorphous precursor route as an example of the design process. Here we consider first, the effects of alloy composition on intrinsic magnetic properties. This is followed by consideration of alloying additions necessary to produce an appropriate amorphous precursor. Typical experimental steps used to identify the structure and properties of the resulting materials are also illustrated.

2.2.1 Stages of Evolution of Microstructure

The amorphous alloys in the form of thin ribbons prepared by rapid solidification technique using melt-spinning machine appeared to be the most suitable method available until now to synthesize nanocrystalline alloys with attractive soft magnetic properties. The basic principle for the crystallization method from amorphous solids is to control the crystallization kinetics by optimizing the heat treatment conditions such as annealing temperature and time, heating rate, etc. So that the amorphous phase crystallizes completely in to a polycrystalline material with ultrafine crystallites nanocrystallization can be realized upon either isothermal or an isothermal annealing in various amorphous metallic alloys in the form of ribbons. Controlled crystallization of FINEMET type of Fe-Cu-Nb-Si-B alloys can be used to obtain partially crystallized materials with nanometer size crystallite embedded in residual amorphous matrix. These special nanocrystal/amorphous composite structures with appropriate compositions allow the material to exhibit extraordinary soft magnetic properties [2.12-2.15].

FINEMET alloys crystallized at temperature above their primary crystallization temperature but below the secondary crystallization temperature can yield nanocrystalline grains with average grain size 10-50nm as a result of primary crystallization of α-Fe (Si) phase embedded in a still remaining amorphous matrix. The excellent soft magnetic properties only occur when the grain size of primary crystallization product of α-Fe (Si) is limited to 10-15nm.The nanocrystalline microstructure and the accompanying soft magnetic properties are rather insensitive to the precise annealing conditions within a wide range of annealing temperature Ta ≈ 525-580^{o}C. They develop in a relatively short period of time (about 10~15 minutes) and do not much latter even after prolonged heat treatment of several hours [2.14].

Only annealing at more elevated temperature above about 600°C leads to the precipitations of small fractions of boride compounds like Fe_2B or Fe_3B with typical dimensions of 50nm to 100nm, while the ultra-fine grain structure bcc Fe-Si still persists. Further increase of the annealing temperature above about 700°C finally yields grain coarsening. Both the formation of Fe brodies and grain coursing deteriorates the soft magnetic properties significantly. The evolution of microstructure during annealing is depicted schematically in Figure 2.2 and summarized as follows according to Hono *et. al.* [2.16-2.17]. Formation of the nanocrystalline microstructure in the amorphous phase was depicted by G. Herzer in 'the nanocrystalline soft magnetic alloys' [2.18].

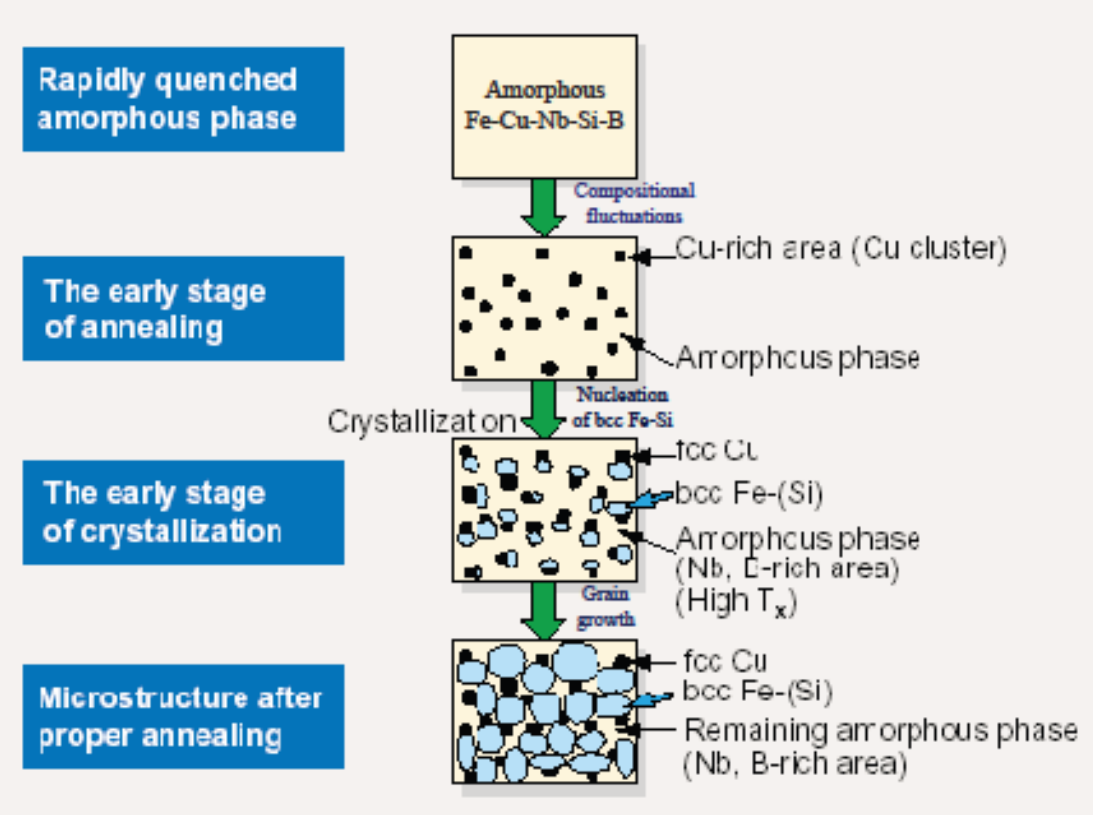

Fig.2.2 Schematic illustration of the formation of nanocrystalline structure

The formation of the particular nanocrystalline structure is essentially related to the combined addition of Cu and Nb (or other group IV or VI elements) and their low solubility in Fe-Si (<0.2 at % Cu, <0.1 at % Nb). Copper enhances the nucleation of bcc grains while Nb impedes grain coarsening and at the same time, inhibits the

formation of Boride compounds. The microstructure evolution is schematically illustrated in Figure 2.2 can be summarized as follows.

Thus the regions in between the Cu rich clusters provide a significantly increased density of nucleation sites for the crystallization of bcc Fe. The consequence is an extremely fine nucleation of bcc Fe-Si crystallites at a high rate, which subsequently grow in a diffusion-controlled process as the annealing proceeds furthers. As annealing goes on the grain size of the α-Fe(Si) increases. At the same time the Si content of this phase keeps increasing since Si tends to be partitioned to the bcc α-Fe(Si) phase. Since the Nb and B enrichment in the amorphous phase stabilizes the remaining state, the grain growth of the bcc phase eventually stops. The presence of Nb at the same time inhibits the formation of Fe-B compounds. The Cu concentration of the clusters also increases as the crystallization proceeds.

At the optimum stage, three distinct phases are present based on the chemical composition. As the bcc Fe-Si phase forms, Nb and B are excluded from the crystallite because of their low solubility in bcc Fe and are enriched in the residual amorphous matrix. At a time all the Si tends effectively to be partitioned into the bcc Fe-Si phase [2.19-2.20]. The particular enrichment with B and Nb increasingly stabilizes the residual amorphous matrix, thus, hiders coarsening of the bcc grains. The presence of Nb at the time inhibits the formation of Fe Boride compounds. The transformation finally ceases in a metastable two-phase microstructure of bcc Fe-Si embedded in an amorphous Fe-Nb-B matrix.

2.2.2 Advantages of Soft Nanocrystalline Alloys

Nanocrystalline amorphous ribbons are produced by the melt-spinning technique to produce an amorphous metal and then heat treating this alloy at temperature higher than its crystallization temperature. The choice of soft magnetic materials for applications has been guided by recent developments in the field of soft magnetic materials. Amorphous and nanocrystalline magnetic materials, in terms of combined induction and permeability are now competitive with Fe-Si bulk alloys and the Fe-Co alloys. In Figure 2.3 [2.21], figures of merit for Fe-based amorphous alloys, Co-based amorphous alloys and nanocrystalline alloys are summarized. Co-based amorphous alloys, Fe-based amorphous alloys and nanocrystalline alloys have evolved over the past decades with soft magnetic properties which now exceed those of the bulk alloys based on Fe, Co and Fe-Co.

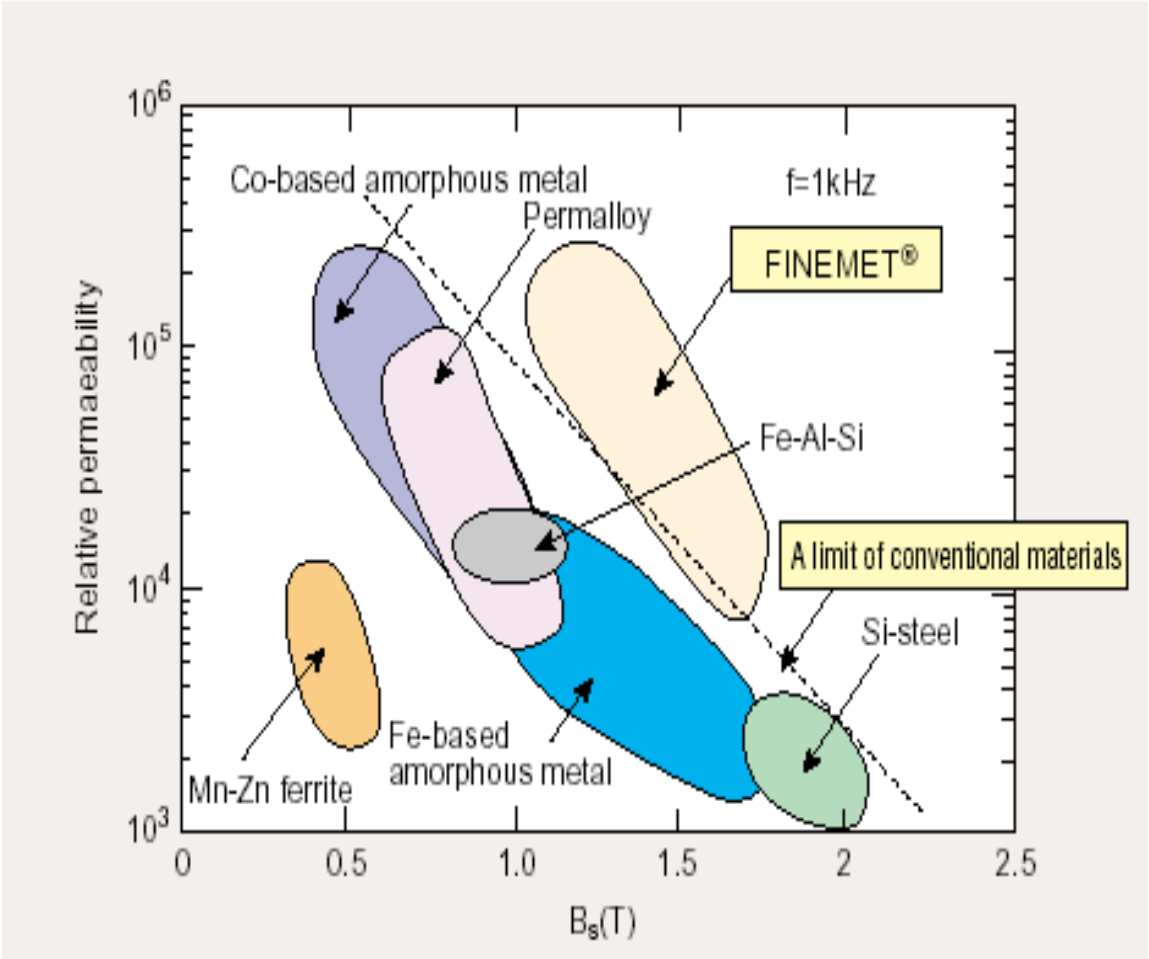

Figure 2.3 FINEMET is superior compared to conventional materials

This FINEMET material is still in its immaturity since its emergence, although much research work has been carried out for the potential utility of this unique material.

At the stage of development, this material has the following advantages:

- High saturation magnetic flux density more than 1 Tesla or 10 kOe.
- High permeability over $\mu_i \approx 10{,}000$ at 100 kHz.
- Excellent temperature characteristics.
- Less affected by mechanical stress.
- Audio noise emission is very low, lower magnetostriction significantly reduces audible noise emission when the voltage and current is applied to the core at audible frequency range.

- Flexible to control the magnetic properties, "B-H curve shape" during the annealing, and three types of B-H curve squareness, high, middle and ion resonance ratio, corresponding to various application.

2.3 Conditions for the Formation of Nanocrystalline Alloys

The essential conditions for preparing of nanocrystalline materials are.

(i) The magnetic properties are highly dependent on the grain size; if the grain size is larger; the magnetic anisotropy would be very high, which is turn will have diverse effect on the soft magnetic properties specially the permeability.

(ii) For the crystallization process there should be nucleation centers initiated to be distributed throughout the bulk of amorphous matrix.

(iii) For stabilizing the crystallites there must be a nucleation.

(iv) Nanocrystalline materials obtain from crystallization must be controlled that crystallites do not grow too big. The grain growth should be controlled so that the grain diameter is within 15-20nm.

(v) The size of the grain can be limited to nanometer scale by doping group-II metals are

→ Cu (Au ……)

→ Nb, W, Mo, Cr, Ta etc.

(vi) The stability must be lower and the crystallization must be higher.

There is additional understanding of the unusual properties possessed by nanophase materials; there are three other associated areas, which need serious attention:

- Identification and development of suitable preparation methods, especially which are capable of providing large industrial quantities of nanometer scale.
- For manufacturing of these materials processing methods should be develop useful size and shape without losing their nanometer size feature.
- Identification of proper crystallization methods, where the nanometer size range of these materials falls just below or at the resolution limit of the conventional tools.

2.4 Stability of the Amorphous and Nanocrystalline Materials

Amorphous materials are always metastable state which leads to transform into more stable crystalline phase. There are three kinds of stability of significance for magnetic ribbons;

(i) Their resistance to the initiation of crystallization.

(ii) Structural relaxation effect, and

(iii) The relaxation or reorientation of directional order.

At temperature below the crystallization temperature, structural relaxation takes place due to atomic rearrangement. It is very difficult to get pure metals in the amorphous state. It is necessary to add glass forming materials to pure metals or alloys to get amorphous state and to bring cooling rate within a reasonable rate. Usually around 20% glass forming materials like B, Si, P, C etc. within a which have atomic radii comparatively small compared to those of metallic atoms occupy the voids left between the bigger atoms of metals when they are closely packed. It can be showed that when there is random close packing of hard spheres, there is about 20% voids created between these atoms.

The glass forming materials the melting point of the alloys and thereby the separation between the glass forming temperature and the crystallization temperature is reduced. The formation and the resultant stability of amorphous alloys are important topic both for theoretical understanding and technically. The theoretical analyses of the factors controlling the case of formation and the stability of the resultant amorphous alloys have been extensively reviewed [2.22 - 2.23]. From the thermodynamic view point [2.24 - 2.25], the ability of an alloy to be quenched into the glassy state is generally measured by the magnitude of the quantity.

$$\Delta T_g = T_m - T_g \qquad (2.1)$$

Where T_m and T_g are the melting and glass temperature respectively. The stability of the glass after formation in a similar manner is generally measured by the magnitude of the quantity.

$$\Delta T_x = T_x - T_g \qquad (2.2)$$

Where T_x is the temperature for the onset of crystallization. As the temperature decrease from T_m, the rate of crystallization will increase rapidly but then fall rapidly as the temperature decrease below T_g. The amorphous alloy composition most

favorable for glass formation is near eutectic i.e. the composition in which the transformation from the liquid state to solid state takes place instantaneously without passing through liquid plus solid mixed phase. The deeper the eutectic the better is the glass formation ability [2.26]. There have been three approaches for relating the stability of the glass, i.e. its microstructure:

(i) Barnaul's model of randomly packed hard sphere's [2.27]. The atoms of the metal are assumed to from a random network of close packed hard spheres and the smaller metalloid atoms fill the holes inherent in such structure.

(ii) The effect of atomic sizes and inter atomic interactions [2.28], i.e. Chemical bonding suggested that it is chemical bonds which are dominating factors in glass formation and stability.

(iii) The third approach [2.29] is based on the role of the electron gas and showed that under certain circumstances a nearly free electron gas will produce a barrier against crystallization.

The transition to the glassy state and the crystalline state is accompanied by an exothermic heat effect giving rise to a sharp peak in temperature dependence of the heat flow. Therefore, DTA is a widely used technique to study thermally induced transformations in amorphous alloys and to determine T_g and T_x. The magnitude of T_g and T_x are very different for amorphous materials and depend strongly on composition. The activation energy ranges typically between 2 and 6 eV [2.30].

2.4.1 Characteristics of the Glass Transition Temperature

When the time scale of molecular rearrangements occurs glass transition temperature (T_g) are too long for equilibrium to be maintained:

(i) T_g means the time scale of the experiment maters.

(ii) A high frequency/short time scale experiment allows less long for equilibrium to be established – even for an identical cooling rate.

(iii) NMR (high frequency technique 10^{15} Hz.) always measures a higher T_g than DTA (1 Hz.).

(iv) In the glass itself, entropy is similar to the crystal and original in vibrational modes, which are still present.

(v) Long range transitional motions are frozen out. The temperature T_g configuration relaxation (including translational motion) but vibrational relaxations are still in equilibrium.

(vi) T_g decreases as melt cooled more and more slowly.

(vii) When the timescale of the experiment and the configuration relaxation time coincide, begin to see departure from equilibrium.

(viii) The time scale for configuration relaxation will be related to rotational or translational diffusion coefficient.

(ix) Optional definition of T_g is when the viscosity of the super-cooled liquid exceeds 10^{13} NSm^{-2}. Where as in the liquid there is an Arrhenius type with a Boltzmann factor containing activation energy.

2.4.2 Differential Thermal Analysis and its Application

Differential thermal Analysis (DTA) is an important technique for the study of structural change both in solid and liquid materials under heat treatment. During this process, the temperature difference between a substance and reference material is measured as a function of temperature whilst the subject and the reference material are subjected to some controlled temperature program. The transition of an amorphous or glassy state to crystalline state is accompanied by an exothermic heat effect that gives rise to a sharp peak in temperature dependence of the heat flow. To study this thermally induced transformation in amorphous alloys, DTA is a widely used technique. DTA detects the release or absorption as they are heated or cooled. Such information is essential for understanding thermal properties of materials. Analysis of decomposition of glass materials, crystalline phase charges, chemical reactions and glass transition temperature are some of the properties with DTA.

Amorphous alloys are in a metastable state and tend to transition into stable crystalline phases. At temperature below the crystallization temperature, structural relaxation effect takes place which are caused by atomic rearrangements. DTA is an important technique for the study of structural change both in solid and liquid materials under heat treatment. The principle of DTA is widely used to understand the crystallization nature of the amorphous. Differential thermal analysis is a direct and effective technique for analyzing the kinetics of amorphous materials and stability with respect to crystallization process.

The crystallization is associated with the nucleation and growth process. Since the formation of an amorphous alloy depends on the absence of LRO, change of composition is expected to affect T_g and T_x. This is because long range ordering of atoms depends on the free energy difference between the crystalline state and the amorphous state. The magnitude of T_g and T_x are very different for amorphous materials and depend strongly on composition. Using DTA technique it is possible to determine T_g and T_x. Nanocrystalline amorphous ribbons prepared by rapid quenching method have been subjected to DTA using a Shimadzu Thermal Analyzer. Different peaks, crystallization temperatures, crystallization activation energies are obtained from this analysis.

2.4.3 Evaluation of Activation Energy Based on DTA Technique

Based on the work of Murray and White [2.31 – 2.33], the kinetics of materials can be understood by interpretation of DTA patterns of the materials. The dependence of T_x on the heating rate $\beta = \frac{dT}{dt}$ can be used to determine the activation energy of crystallization [2.34]. Considering the fraction x of amorphous material transformed into the crystalline state in time t and at temperature T obtains for the first-order rate process [2.35 - 2.36]

$$\left(\frac{\delta x}{\delta t}\right)_T = K(1-x) \tag{2.3}$$

For thermally activated process, the rate constant K obeys an Arrhenius type of equations

$$K = K_o e^{-\left(\frac{\Delta E}{RT}\right)} \tag{2.4}$$

where K_o is a constant and ΔE is the activation energy. Combining equation (2.3) and (2.4) and using $dx = \left(\frac{\delta x}{\delta t}\right)_T dt + \left(\frac{\delta x}{\delta t}\right)_t dT$ with $\left(\frac{\delta x}{\delta t}\right) dt \cong 0$, are obtains

$$\frac{dx}{dt} = K_o(1-x)e^{-\left(\frac{\Delta E}{RT}\right)} \tag{2.5}$$

$$\frac{d^2x}{dt^2} = \frac{d}{dt}\left[K_o(1-x)e^{-\left(\frac{\Delta E}{RT}\right)}\right]$$

$$= -K_o\frac{dx}{dt}e^{-\left(\frac{\Delta E}{RT}\right)} + K_o(1-x)\frac{d}{dT}\left\{e^{-\left(\frac{\Delta E}{RT}\right)}\right\}\frac{dT}{dt}$$

$$= -K_o \frac{dx}{dt} e^{-\left(\frac{\Delta E}{RT}\right)} + \frac{dx}{dt}\left(\frac{\Delta E}{RT^2}\right)\beta$$

At the peak of the exothermic heat, the change of the reaction rate $\frac{d^2x}{dt^2} = 0$, yielding with T = T_x but $\frac{dx}{dt} \neq 0$

$$K_o e^{-\left(\frac{\Delta E}{RT_x}\right)} = \left(\frac{\Delta E}{RT_x{}^2}\right)\beta \qquad (2.6)$$

From equation (2.6) it is easily seen that

$$\frac{d\left(ln\frac{\beta}{T_x^2}\right)}{d\left(\frac{1}{T_x}\right)} = -\frac{\Delta E}{R} \qquad (2.7)$$

Here $\beta = \frac{dT}{dt}$ the heating rate. ΔT_x for the stability of amorphous alloys as given by equation (2.5) and is obtained from DTA. Similar correlation between thermal stability as measured by ΔT_x and ΔE appears too small.

From the measured data of the heating rate (β) and the respective crystallization temperature (ΔT_x), the activation energy can be deduced from the slope of a plot $ln\frac{\beta}{T_x^2}$ versus $\frac{1}{T_x}$from equation (2.7) can be derived from transformation theory, where ΔE is the activation energy for versus flow and other terms have been omitted because they an insignificant temperature dependence in this region of temperature. The values of ΔE also appear to correlate well with the number of atomic species in the alloy; the more complex the alloy the grater is ΔE.

2.5 Determination of Nanometric Grain Size by X-Ray Diffraction

Nanocrystalline alloys are basically crystalline and because of their crystallinity and they exhibit Bragg scattering peaks in X-ray diffraction experiments. However, due to their small size, significant fine particle broadening is observed in the Bragg peaks. The X-ray scattering from a crystalline solid is given by Bragg's law:

$$2d \sin\theta = n\lambda \qquad (2.8)$$

This equates the path difference scattered from parallel crystalline planes spaced d = d_{hkl} apart to an integral number (n) of X-Ray wavelength λ. Here θ is the X-Ray angle of incidence (and of diffraction) measured with respect to the crystalline planes. Bragg scattering occurs at discrete values of 2θ satisfying the Bragg condition for an

infinite crystal, i.e. Bragg peaks are δ-functions. The peaks are broadened over a range of angles for finite sized crystals as shown in Figure 2.4.

The better understand of the phenomenon of fine particle broadening following argument of Cullity [2.37] is outlined below. We consider a finite crystal of thickness, D_g = md, where is an integer and d is the distance between crystalline planes, i.e., there are m planes in D_g. considering Figure 2.5, if the broadened Bragg peak begins at an angle $2\theta_2$ and ends at $2\theta_1$, the breadth of the peak or full width at half maximum is given as:

$$\beta = \frac{1}{2}(2\theta_1\text{-}2\theta_2) = \theta_1\text{-}\theta_2 \qquad (2.9)$$

Now consider the path differences for each of the two angles $\theta_1$andθ_2, for X-rays travelling the full thickness of the crystal. The width β is usually measured in radians; intensity is equal to half the maximum intensity. As a rough measure of β , we can take half the difference between the two extreme angles at which the intensity is zero, which amounts to assuming that the diffraction line triangular in shape.

We now write the path difference equations for those two angles related to the entire thickness of the crystal rather to the distance between adjacent planes.

$$2D_g \sin\theta_1 = (m+1)\lambda \qquad (2.10)$$

$$2D_g \sin\theta_2 = (m-1)\lambda \qquad (2.11)$$

By the subtraction;

$$D_g\,(\sin\theta_1 - \sin\theta_2) = \lambda \qquad (2.12)$$

$$2D_g \cos\left(\frac{\theta_1+\theta_2}{2}\right)\sin\left(\frac{\theta_1-\theta_2}{2}\right) = \lambda \qquad (2.13)$$

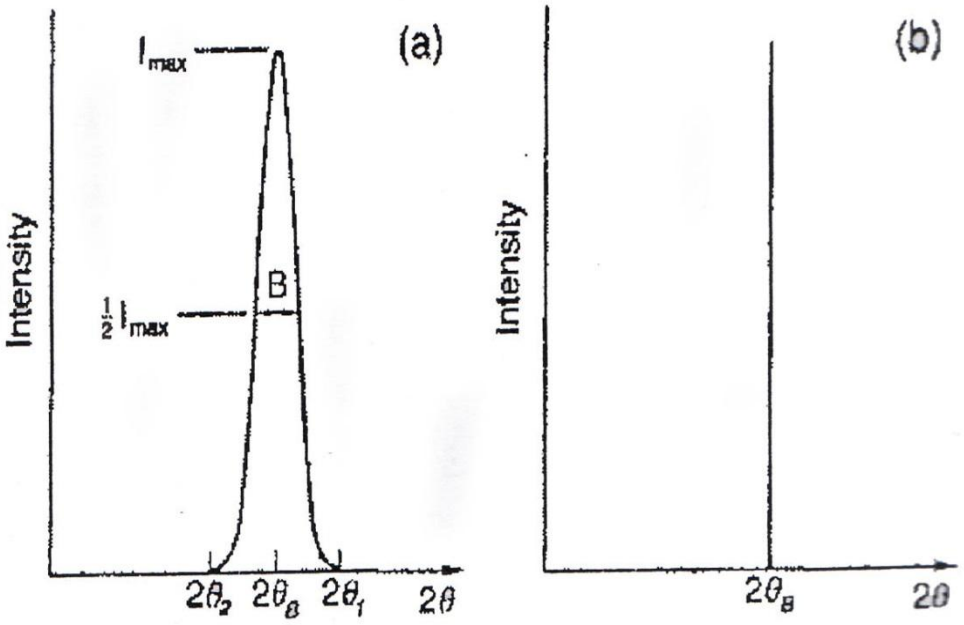

Figure 2.4 Effect of fine particle broadening in XRD (a) fine particle and (b) perfect crystal

But θ_1 and θ_2 are both very nearly equal to θ, so that $\theta_1 + \theta_2 \approx 2\theta$ and $\sin\left(\frac{\theta_1-\theta_2}{2}\right) \approx \left(\frac{\theta_1-\theta_2}{2}\right)$ thus the equation(2.13) can be written as:

$$2D_g \cos\theta.\left(\frac{\theta_1-\theta_2}{2}\right) = \lambda \tag{2.14}$$

From the equation (2.9) and equation (2.14) we get:

$$\beta.D_g\cos\theta = \lambda \tag{2.15}$$

$$D_g = \frac{\lambda}{\beta cos\theta} \tag{2.16}$$

A more exact empirical treatment yields:

$$D_g = \frac{0.9\lambda}{\beta cos\theta} \tag{2.17}$$

This is known as the Scherer's formula. It is used to estimate the particle size of very small crystals from the measured width of their diffraction curves.

2.6 Magnetic Dipole Moments and Magnetization

The vast majority of soft magnetic materials have one or more of the ferromagnetic transition metal elements Fe, Co or Ni, or the rare earth metal Gd as a

majority component. The vast majority of soft magnetic materials have one or more of the ferromagnetic transition metal element. The magnetic dipole moments of the elemental and alloy magnets are almost completely understood through the Band Theory of Solids [2.38]. The band theory of solids considers the broadening of localized atomic states with discrete eigen values into a continuum of states for more itinerant electrons over arrange of energies. The theory allows for calculation of energy dispersion (i.e. energy as a function of wave vector) and orbital angular momentum specific and spin-resolved densities of states. Among the success of the band theory descriptions of magnetic properties are:

(i) The prediction of non-integral of half integral atomic dipole moments and resulting ground state magnetization in the metals and alloys.

(ii) The prediction that band widths and exchange splitting (energy differences between spin up and spin down bands) are intimately dependent on magnetic coordination number and atomic volume.

In densities of states are more structures within free electron model and in more accurate description of the magnetic states in solids. The results of band theory, in describing alloying affects on magnetic dipole moment in solid. The variation of the mean atomic magnetic dipole moment as a function of composition in the transition metal alloy system. Spin resolved densities of states $g_{+}(E)$ and $g_{-}(E)$ for Co and Fe atoms, in an equi-atomic Fe Co alloy, as a function of energy (where the Fermi energy, E_F is taken as the Zero of energy). The number of spin up, n_{+} and spin down, n_{-} electrons in each band can be calculated again by integrating these densities of state:

$$n_{+} = \int_0^{E_F^{+}} g_{+}(E)dE \qquad (2.18)$$

and $$n_{-} = \int_0^{E_F^{-}} g_{-}(E)dE \qquad (2.19)$$

Here the Fermi energies, E_F, are the same and the zero's of energy are different for the two spin bands and the atom resolved (i.e. Fe and Co) magnetic dipole moments can be calculated as:

$$\mu_m = (n_{+} - n_{-})\mu_B \qquad (2.20)$$

Knowledge of atomic values or alloy density, then allows for the direct calculation of the alloy magnetization

Table 2.1, summarizes the absolute zero and room temperature (where applicable) magnetizations and atomic dipole moments for some important transition metal and rare earth elemental magnets. Also shown Curie temperatures i.e. ferromagnetic ordering temperatures which are not ground state properties that directly calculable from the band theory [2.39].

Table 2.1 Spontaneous and room temperature magnetizations, magnetic dipole moments and Curie temperature for elemental ferromagnets

Element	$\mu_m@0K(\mu_B)$	$M_s@0K$ (G)	$M_s@RT$ (G)	$T_c(K)$
Fe	2.22	1740	1707	1043
Co	1.72	1446	1400	1388
Ni	0.606	510	485	627
Gd	7.63	2060	--	292
Dy	10.2	2920	--	88

2.6.1 Magnetization of the Nanocrystalline Ribbon

The saturation magnetization of a material at a temperature of 0 K is one of its basic properties. Measurements are usually expressed as average moment per magnetic atom in units of the Bohr magnetron, μ_b as specific saturation magnetization for the amorphous alloy, σ_s in units for Am^2/kg. The moments of most amorphous alloys are lower than those of the structural disorder on the moments is very small.
This, points out the importance of chemical instead of structural disorder. The reduction is least in B-based and highest in p-based glass. The observed moments on TM-M glasses can approximately fitted to a formula [2.38].

$$\mu = \left(\frac{\mu_{TM} C_{TM} - C_B - 2C_{sc} - 3C_\rho}{C_{Tm}} \right) \qquad (2.21)$$

Where μ_{TM} is the magnetic moment of TM-M atoms, taken as 2.6, 1.6 and 0.6 respectively in Bohr magneto for Fe, Co and Ni. C's are respective concentrations. This clearly demonstrates the change transfer from metalloid to d-band of transition metal and seems to suggest that 1, 2 or 3 electrons are transferred from each of B, Si

(C, Ge) or P atom. The relative number of electrons donated can be listed as – $P_{13}C_7$ > -$S_{15}B_{10}$ > -$P_{16}B_6AI_3$ > -$P_{14}B_{13}$ > -B_{20} Based on the relative magnitudes of M_s.

2.6.2 Ferromagnetic ordering (Curie) Temperatures

Ferromagnetism is a collective phenomenon since individual atomic moments interact so as to promote alignment with one another. This collective interaction gives rise to the temperature dependence of the magnetization. Two models have explained the interaction between atomic moments. Mean Field Theory considers the existence of a non-local internal magnetic field, called the Weiss field, which acts to align magnetic dipole moments even in the absence of an applied field H_a. Heisenberg Exchange Theory considers a local (usually nearest neighbor) interaction between atomic moments (spins) which acts to align adjacent moments even in the absence of a field.

The basic assumption of the mean field theory is that this internal field is non-local and is directly proportional to the sample magnetization.

$$H_{INT} = \lambda_W M \tag{2.22}$$

Where the constant of proportionality, λ_W, is called the Weiss molecular field constant.

To consider ferromagnetic response in applied field, H_a, as well as the randomizing effects of temperature, we consider the superposition of the applied and internal magnetic fields. By analogy with the problem of paramagnetic moments, the average atomic dipole moment can be expressed in terms of the Brillion function

$$<\mu_m> = \mu_m^{atom} B_J(\alpha') \tag{2.23}$$

where $\alpha' = -\left(\frac{\mu_0 \mu_m^{atom}}{K_B T}\right)(H + \lambda_W M)$ for a collection of classical dipole moments. The saturation magnetization

$$M_S = N_m <\mu_m^{atom}> \tag{2.24}$$

$$\frac{M}{N_m \mu_m^{atom}} = \frac{M}{M_s} = B_J\left[H + \lambda_w M\right] \tag{2.25}$$

Under appropriate conditions, this leads to solutions for which there is a non-zero magnetization (spontaneous magnetization) even in the absence of an applied field.

For T > T_c, the ferromagnetic T_c the only solution to equation (2.25) is $M = 0$, i.e., no spontaneous magnetization and thus paramagnetic response. For T < T_c, we obtain solutions with a non-zero, spontaneous magnetization, the defining feature of a ferromagnet.

The Heisenberg model considers ferromagnetism and the defining spontaneous magnetization to result from nearest neighbor exchange interactions, which acts to align spins in a parallel configuration, instead of a non-local, mean field. Consider Heisenberg ferromagnet; assume that the atomic moments due to a spin vector S on nearest neighbor sites are coupled by a nearest neighbor exchange interaction that gives rise to a potential energy

$$E_p = -J_{ex} S_i \times S_{i+1}, \qquad (2.26)$$

That for $J_{ex} > 0$ favors parallel alignment of the spins. The exchange suitably scaled, replaces the Weiss molecular field constant in the mean field theory of ferromagnetism to explain the temperature dependence magnetization.

Ferromagnetic exchange interactions set the scale for T_c in ferromagnetic alloys. Inter atomic exchange couplings can be calculated from first principles by considering the energy change associated with rotation of individual spins in the host material. These exchange interactions can be used within a mean field theory to estimate the T_c. In transition metal solids a measure of the overlap between nearest neighbor d-orbital is given by the ratio of the atomic to the 3d ionic (or nearest neighbor) radius. In mean field theory the T_c can be related to the exchange energy as follows:

$$T_C = \frac{2S(S+1)}{3K_B} \sum_{ij} T_{ij} , \qquad (2.27)$$

where S is the total spin angular momentum, K_B is the Boatman's constant and T_{ij} is the exchange interaction between atoms at the position r_i and r_j.

EXPERIMENTAL DETAILS

3.1 Methods used for preparation of Nanocrystalline Alloy

There are various techniques in use to produce a metallic alloy in an amorphous state whose the atomic arrangement has no long range periodicity. The methods are generally classified into two groups:

(i) The atomic deposition methods.

(ii) The fast cooling of the melt.

As we know, controlled crystallization from the amorphous state is the only method which presently available to synthesize nanocrystalline alloys with superior soft magnetic properties. In this thesis work amorphous ribbons have been prepared by fast cooling of the melt.

3.1.1 The Fast Cooling of the Melt

The molten alloy must be cooled through the temperature range from the melting temperature (T_m) to the glass transition temperature (T_g) very fast allowing no time for crystallization. The factors controlling T_g and crystallization are both structural and kinetic. Atomic arrangement, bonding and atomic size effects are related in the structural factors. The structural factors as discussed by D. Turnbull [3.1] are the nucleation, crystal growth rate and diffusion rate compared to the cooling rate. The pioneering work of P. Duwez, *et al* [3.2], number of devices have been reported for obtaining the necessary high quenching rates and producing continuous filaments. The methods using the principle of fast cooling of melt techniques are:

(i) The gun techniques

(ii) Single roller rapid quenching techniques

(iii) Double roller rapid quenching techniques

(iv) Centrifuge and rotary splat quencher techniques

(v) Torsion catapult techniques

(vi) Plasma-jet spray techniques

(vii) Filamentary casting techniques

(viii) Melt extraction techniques

(ix) Free-jet spinning techniques

(x) The melt spinning techniques

Although the different methods used in preparing amorphous metallic ribbons are mentioned here, only the melt spinning technique, which is widely used to prepare the amorphous ribbons.

3.1.2 Master Alloy Preparation

Amorphous ribbon with the composition $Fe_{72.5}Cr_1Nb_3Cu_1Si_{13.5}B_9$ was prepared in an arc furnace on a water-cooled copper hearth under an atmosphere of pure Ar. Their purity and origin of the constituent elements were Fe (99.9%), Cr (99.9%), Nb (99.9%), Cu (99.9%), Si (99.9%) and B (99.9%) as obtained from Johnson Mathey (Alfa Aesar Inc.). The required amounts of the constituent elements were taken from pure metal bars or flakes, weighed carefully with a sensitive electronic balance and placed on the copper hearth inside the arc furnace. Before melting, the furnace chamber was evacuated (10^{-4} torr), and flashed with Ar gas. The process was repeated several times to get rid of residual air and finally the furnace chamber were kept in an Ar atmosphere.

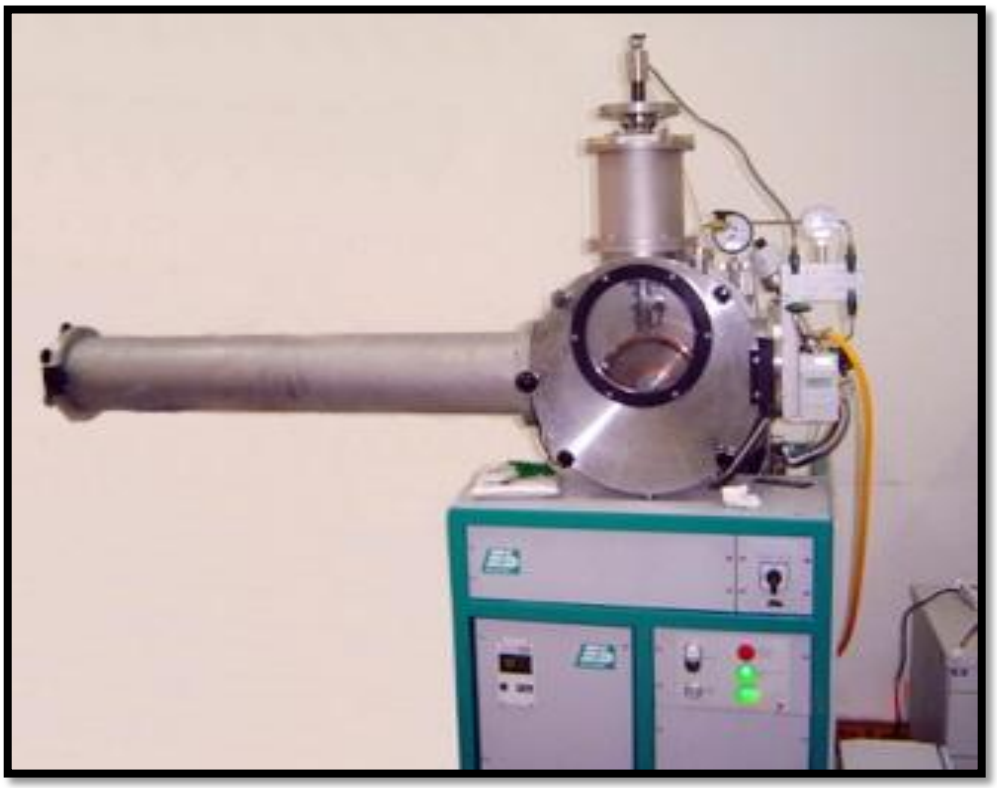

Figure 3.1 Vacuum Arc Melting Machine

A substantial amount of pure Titanium getter, placed inside of the chamber on the side of the copper hearth was melted first in order to observe any oxygen present in the furnace chamber. The constituent elements were then melted in the shape of buttons. The arc melting facilities used to prepare the sample are installed at the Centre for Materials Science, National University of Hanoi, Vietnam. The arc furnace used in the preparation of master alloy is shown in Figure 3.1

3. 1.3 Preparation of Ribbon by Melt Spinning Technique

Melt spinning is a widely used production method for rapidly solidifying materials as well as preparing amorphous metallic ribbon [3.3-3.4]. In order to prepare amorphous of $Fe_{72.5}Cr_1Nb_3Cu_1Si_{13.5}B_9$ alloy, the melt spinning facilities was used at the Centre for Materials Science, National University of Hanoi, Vietnam. The arc melted master alloy was crashed into small pieces and put inside the quartz tube crucible for re-melting by induction furnace using a medium frequency generator with maximum power of 25kW at a nominal frequency of 10kHz.

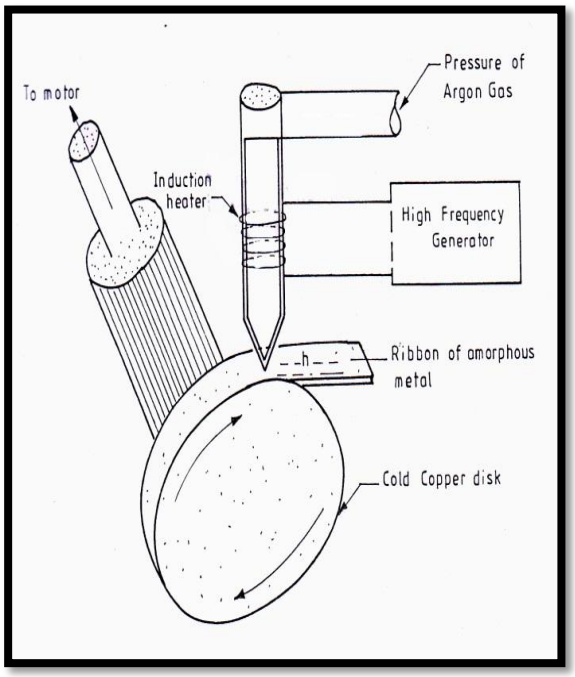

Figure 3.2 Schematic diagram

Figure 3.3 Melt-Spinning Machine

The temperature was monitored by an external pyrometer from the upper surface of the molten alloy through a quartz window. Figure 3.2 shows schematic diagram and Figure 3.3 shows the pictorial view of the Melt-Spinning Machine. The Quartz crucible has in its bottom part, a rectangular nozzle tip of 8 mm length and 0.7

mm width. The position of the nozzle tip can be adjusted with respect to cooper wheel surface, so that the molten alloy was perpendicularly ejected onto the wheel surface from a distance of about 0.3 mm. The small piece of the master alloy samples were inductively remelted inside the quartz tube crucible followed by ejecting the molten metal with an over pressure of 250 mbar of 99.9% pure Ar supplied from an external reservoir through a nozzle onto a rotating copper wheel with surface velocity of 30 m/sec.

The metal alloys were ejected at a temperature of about 150 to 250 K above the melting point of the alloy. The resulting ribbon samples had thickness of about 20-25 μm and width ~6 mm. Processing parameters such as the thermal conductivity of the rotating quench wheel, wheel speed, ejection pressure, thermal history of the melt before ejection, distance between nozzle of quartz tube and rotating wheel, as well as processing atmosphere have influenced on the microstructure and properties of melt-spun ribbons. The lower pressure of 250 mbar as mentioned above stabilizes the turbulence between melt pull and rotating copper wheel enhancing the heat transfer resulting in a more uniform quenching. As a result, a more uniform ribbon microstructure can be obtained at relatively low wheel speed. With increasing wheel speeds for a given ejection rate, the increasing extraction rate results in thinner ribbons.

3.1.4 Important Factors to Control the Thickness of Ribbons

(i) Rotating speed

- Angular velocity ω = 2000rev/min
- Surface velocity V = 20 m/s to 30 m/s

(ii) Gap between nozzle and rotating copper drum (h) = 200 to 30 μm

(iii) Oscillations of the rotating copper drum both static and dynamic has maximum displacement 1.5 to 5 μm

(iv) Pressure = 0.2 to 3.0 bar at argon atmosphere

(v) Temperature of molten metals $T_m \approx 1500^0$C; the temperature did not exceed 1800^0 C otherwise quartz tube would be melted.

(vi) A steady flow of the molten metals on the surface of the rotating drum needs to be ensured.

3.1.5 Confirmation of Amorphousity Ribbons

The amorphous state of the ribbon has been confirmed by X-ray diffraction using D8 ADVANCE XRD, BUKER AXSGMh, German system located at Bangladesh Council of Scientific and Industrial Research (BCSIR).

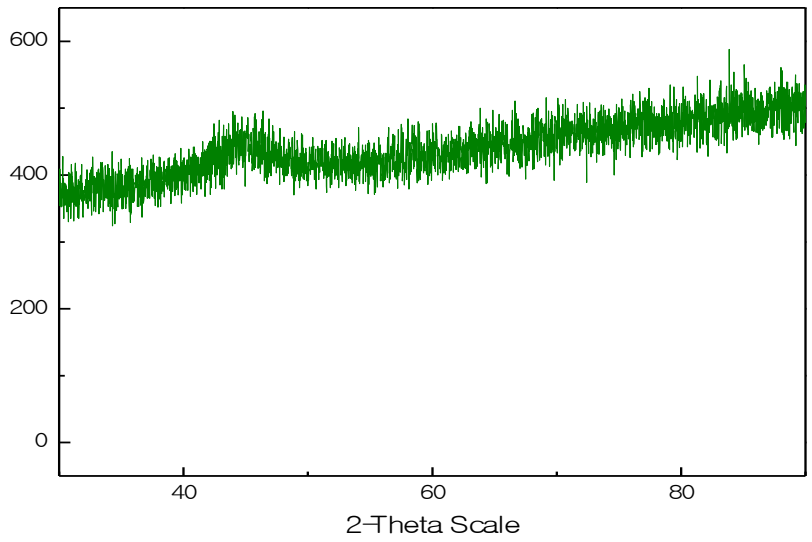

Figure 3.4 X-ray diffraction of as-cast nanocrystalline amorphous ribbons with Composition $Fe_{72.5}Cr_1Nb_3Cu_1Si_{13.5}B_9$

From the X-ray diffraction pattern of the sample in Figure 3.4, there have amorphous peak observed within the scanning range. Although there is a small hump shown in the diffraction pattern around $2\theta = 45^{o}$; but it cannot be regarded due to the crystalline effects. So from all the pattern of X-ray diffraction is confirmed that the samples are in pure amorphous state.

3.2 The Principle of Differential Thermal Analysis

The DTA technique was first suggest by Le Chatelier [3.5] in 1887 and was applied to the study of clays and ceramics. DTA involves heating or cooling a test sample and inert reference under identical conditions, while recording any temperature difference between the sample and reference. DTA is the process of accurately measuring the difference in temperature between a thermocouple embedded in a sample and a thermocouple in a standard inert material such as

aluminum oxide, while both are being heated at a uniform rate. These differences of temperature arise due to phase transition or chemical reactions in the sample involving the evolution of heat or absorption of heat due to exothermic reaction or endothermic reaction measured. The exothermic and endothermic reactions are generally shown data in the DTA trace as positive and negative deviations respectively from a baseline. Then this differential temperature is plotted against time, or against temperature. When a sample and reference substance are heated or cooled at a constant rate under identical environment, their temperature differences are measured as a function of time or temperature as shown by the curve in Figure3.5 (a).

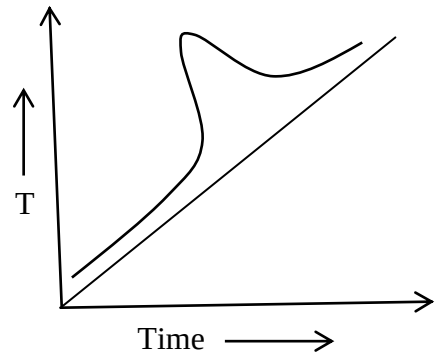

Figure 3.5(a) Heating curve of sample and reference substance

The temperature of the reference substance, which is thermally inactive, rises uniformly when heated, while the temperature of the sample under study changes anomalously when there is physical or a chemical change of the active specimen at a particular temperature. When there is an exothermic reaction there is a peak in the temperature versus time curve, heat released from outside is consumed by the reaction. And when the reaction is over, the sample temperature gradually catch up the temperature of the inactive specimen. The temperature difference ΔT is defined, amplified and recorded by a peak as shown in Figure 3.5 (b).

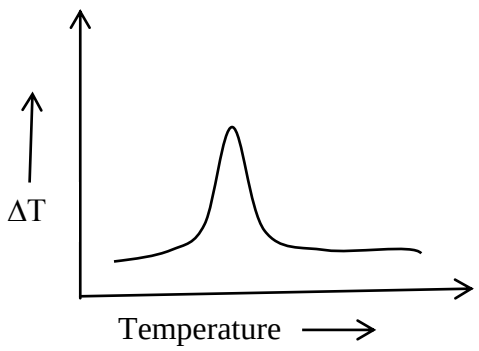

Figure 3.5(b) DTA Curve

For any endothermic reaction or change the active specimen absorbs heat which is reflected in the corresponding trough in temperature versus time curve. Changes in the sample, which leads to the absorption or evolution of heat, can be detected relative to the inert reference. Differential temperatures can also arise between two inert samples when their response to the applied heat treatment is not identical. DTA can therefore be used to study thermal properties and phase changes which do not lead to a change in enthalpy.

Changes in the sample, either exothermic or endothermic, can be detected relative to the inert reference. Thus, a DTA curve provides data on the transformations that have occurred, such as glass transitions, crystallization, melting and sublimation. The baseline of the DTA curve showed then exhibit discontinuities at the transition temperatures and the slope of the curve at any point will depend on the microstructural constitution at that temperature. The area under a DTA peak can be related to the enthalpy change and is not affected by the heat capacity of the sample. DTA may be defined formally as a technique for recording the difference in temperature between a substance and a reference material against either time or temperature as the two specimens are subjected to identical temperature regimes in an environment either heated or cooled at a controlled rate.

3.2.1 Apparatus

The key features of a DTA kit are as shown in Figure 3.6 sample holder comprising thermocouples, sample containers and a ceramic or metallic block, a furnace, temperature programmer, recording system. The essential requirements of the furnace are that it should provide a stable and sufficiently large hot-zone and must be able to respond rapidly to commands from the temperature programmer. A temperature programmer is essential in order to obtain constant heating rates. The recording system must have a low inertia to faithfully reproduce variations in the experimental set-up.

The sample holder assembly consists of a thermocouple each for the sample and reference, surrounded by a block to ensure an even heat distribution. The sample is contained in a small crucible designed with an indentation on the base to ensure a snug fit over the thermocouple bead. The crucible may be made of materials such as Pyrex, Silica, Nickel or Platinum, depending on the temperature and nature of the tests involved. The thermocouples should not be placed in direct contact with the

sample to avoid contamination and degradation, although sensitivity may be compromised. Metallic blocks are less prone to base-line drift when compared with ceramics which contain porosity. On the other hand, their high thermal conductivity leads to smaller DTA peaks.

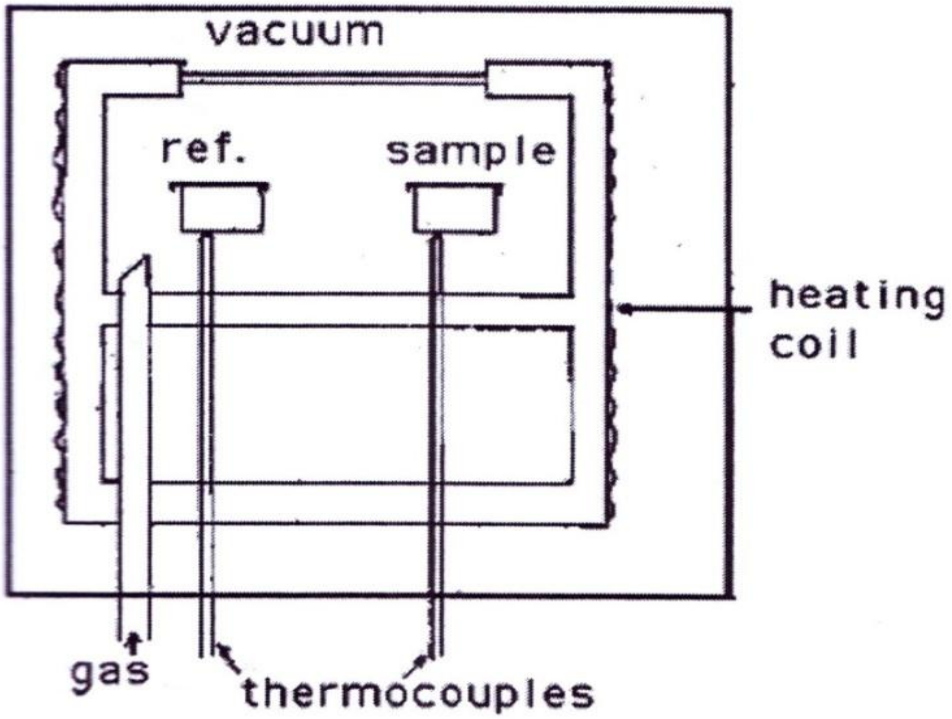

Figure 3.6 Schematic illustration of a DTA cell

The sample assembly is isolated against electrical interference from the furnace wiring with an earthed sheath, often made of platinum-coated ceramic material. The sheath can also be used to contain the sample region within a controlled atmosphere or a vacuum. The specimen holder is placed in the cavity of the heating block which is operated in the center of the cylindrical refractory tube of an electrical furnace. This supplies is a uniform heating rate. The furnace is peaked with calcined china clay. The input of current into the furnace is secured through the secondary of a Variac transformer, which controls the currents. Fine Chromelalumel wires (28 gauges) are used for thermocouples. A cold junction is used for thermocouple leads and the e.m.f. is recorded almost continuously, while the temperature of the inert material is measured at 3 minute intervals. It is essential to use perfectly dry materials, as otherwise errors will be introduced in the analysis. Approximately 0.1 gm anhydrous alumina is used in the reference cup and the sample weight varies over a range 0.05 to 0.125 gm; depending on their density. A heating rate of 10^{o}C to 60^{o}C

per minute of the furnace is conveniently chosen and this gives satisfactory results in most case. A block diagram of DTA as shown in Figure 3.7

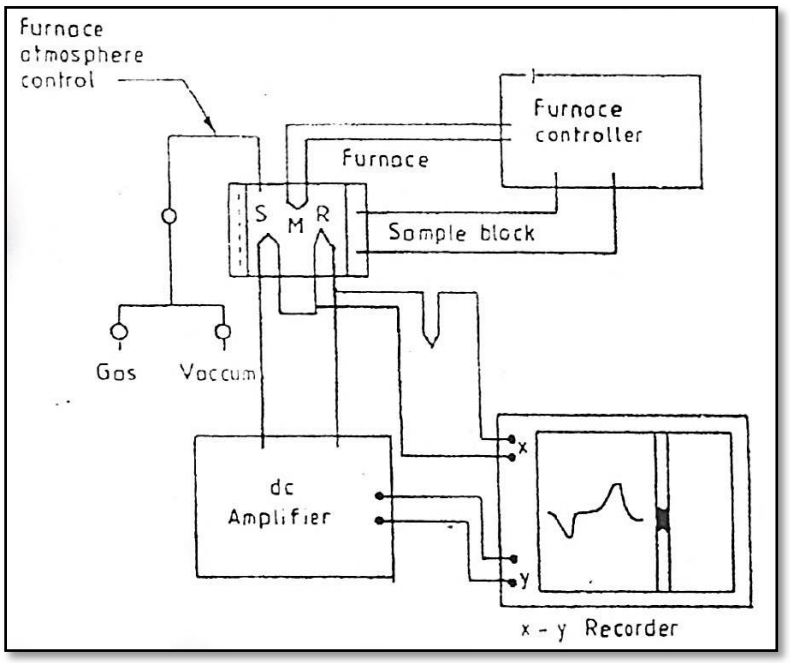

Figure 3.7 Block diagram of a DTA equipment, (S) sample thermocouple, (R) Reference thermocouple, (M) Monitor thermocouple

During experiments a temperature problems are encountered in transferring heat uniformly away from the specimen. These may be mitigated by using thermocouples in the form of flat discs to ensure optimum thermal contact with the new flat-bottomed sample container, made of aluminum or platinum foil. To ensure reproducibility, it is then necessary to ensure that the thermocouple and container are consistently located with respect to each other.

3.3 Experimental Factors

It is necessary to selecting the experimental parameters. For example, the effects of specimen environment, composition, size and surface to volume ratio all affect powder decomposition reactions, whereas these particular variables may not affect solid state phase changes. Experiments are frequently performed on powders so the resulting data may not be representative of bulk samples, where transformations may be controlled by the build-up of strain energy. The packing state of any powder

sample becomes important in decomposition reactions and can lead to large variations between apparently identical samples.

In some circumstances, the rate of heat evolution may be high enough to saturate the response capability of the measuring system; it is better than to dilute the test sample with inert material. For the measurement of phase transformation temperatures, it is advisable to ensure that the peak temperature does not vary with sample size. The shape of a DTA peak does depend on sample weight and the heating rate used. The influence of heating rate on the peak shape and disposition can be used to advantage in the study of decomposition reactions, but for kinetic analysis it is important to minimize thermal gradients by reducing specimen size or heating rate.

3.3.1 Interpretation and Presentation of DTA

There are difficult with the measurement of transition temperatures using DTA curves. The onset of the DTA peak in principle gives the start-temperature, but there may be temperature lags depending on the location of the thermocouple with respect to the reference and test samples or the DTA block. It is wise to calibrate the apparatus with materials of precisely known melting points. The peak area (A), which is related to enthalpy changes in the test sample, is that enclosed between the peak and the interpolated baseline. When the differential thermocouples are in thermal, but not in physical contact with the test and reference materials, it can be shown that A is given by,

$$A = \frac{mq}{gk} \tag{3.1}$$

where m is the sample mass, q is the enthalpy change per unit mass, g is a measured shape factor and k is the thermal conductivity of sample.

With porous, compacted or heaped samples, the gas filling the pores can alter the thermal conductivity of the atmosphere surrounding the DTA container and lead to large errors in the peak area. The situation is made worse when gases are evolved from the sample, making the thermal conductivity of the DTA-cell environment different from that used in calibration experiments. The DTA apparatus is calibrated for enthalpy by measuring peak areas on standard samples over specified temperature ranges. The calibration should be based upon at least two different samples, conducting both heating and cooling experiments.

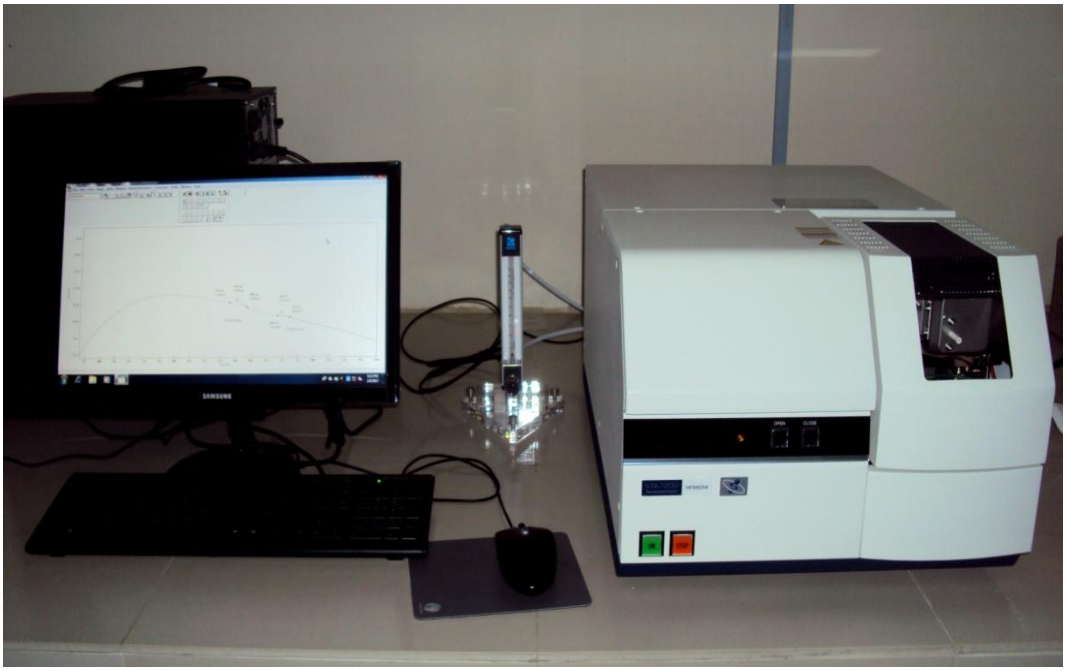

Figure 3.8 TA7000 Series Simultaneous Thermogravimetric Analyzer

In the present work, HITACHI Instruments TA7000 Series Simultaneous Thermogravimetric Analyzer TG/DTA/DSC which is situated at Khulna University of Engineering & Technology (KUET) has been used for thermal analysis shows in Figure 3.8. The Thermo gravimetric/Differential Thermal Analyzer (TG/DTA) combine the flexibility of DTA with the proven capabilities of the TG measurement technology, providing property information for a verity of samples. Thus simultaneous TG/DTA/DSC system can be used for such application as oxidation, heat resistance, and the amount of water, compositional analysis and measurement of ash contents in a sample. This system is also used to cover such need as reaction rate and accelerated degrading tests.

The thermal analysis runs generally for 1 to 1.5 hrs. Thermal analysis curves are obtained by plotting heating temperature and the difference between the temperature of the test and reference substances. From these plots the reaction temperature could be determined. Under standard conditions of the experiment; characteristic curves for the composition of $Fe_{72.5}Cr_1Nb_3Cu_1Si_{13.5}B_9$ nanocrystalline amorphous ribbons. T_{x_1} and T_{x_2} points are indicating the sharp exothermic peaks.

All experiments are run at atmospheric pressure in continuous flow of purified inert gases, Nitrogen. Gases are normally purged into the furnace chamber at the lower end through a purification train in which oxygen and water are removed by

heated copper wool and exhausted from the top into a condensate trap for collecting the condensable volatile products.

A.The Features are:

(i) The TG/DTA can operate in either DSC or DTA mode. In DSC mode it displays heat flow signal.

(ii) The horizontal differential balance provides high sensitivity and accuracy.

(iii) Gas control unit automatically control the environment of the furnace between measurements.

(iv) Auto sampler with 30 samples positions provides laboratory automation and increase productivity.

(v) Through the utilization of an automatic cooling unit, the instrument is now automatically cooled to a set temperature after measurements, which raises the effectiveness of measurements.

B. Specification:

Temperature Range : Room temperature to 1500°C (normally around 1300°C)

Balance Method : Horizontal differential type

Maximum sample weight : 200mg;

Program rate : 0.01 to 100°C/min

Automatic Cooling unit : Force Air Cooling

Gas flow rate : 0 to 1000ml/min

Cooling rate : less than 15 min from 1000 to 50°C

Atmosphere : Air, Inert gas, Vacuum (10^{-2} Torr)

Sample pan material : Platinum, Alumina and Aluminum.

TG measurement Range/Sensitivity: 200 mg /0.2µg

DTA measurement / Sensitivity: +1000µV/ 0.06µV

3.3.2 Annealing

Annealing in metallurgy and materials science, is heat treatment wherein a material is altered, causing changes in its properties such as strength and hardness. It is a process that produces conditions by heating to above the critical temperature, maintaining a suitable temperature, and then cooling. Annealing is used to induce ductility, soften material, relieve internal stresses, refine the structure by making it homogeneous, and improve cold working properties.

In the cases of copper, steel, silver and brass, this process is performed by substantially heating the material (generally until glowing) for a while and allowing it to cool. Unlike ferrous metals, which must be cooled slowly to anneal, copper, silver and brass can be cooled slowly in air or quickly by quenching in water. In this fashion the metal is softened and prepared for future work such as shaping, stamping, or forming.

Annealing occurs by the diffusion of atoms within a solid material, so that the material progresses towards its equilibrium state. Heat is needed to increasing the rate of diffusion by providing the energy needed to break bonds. The movement of atoms has the effect of redistributing and destroying the dislocations in metals and (to a lesser extent) in ceramics. This alternation in dislocations allows metals to deform more easily, so increases their ductility.

3.3.3 Stages

There are three stages in the annealing process, with the first being the recovery phase, which results in softening of the metal through removal of crystal defects (the primary type of which is the linear defect called a dislocation) and the internal stresses which they cause. Recovery phase covers all annealing phenomena that occur before the appearance of new strain-free grains. The second phase is recrystallization, where new strain-free grains nucleate and grow to replace those deformed by internal stresses. If annealing is allowed to continue once recrystallization has been completed, grain growth will occur, in which the microstructure starts to coarsen and may cause the metal to have less than satisfactory mechanical properties.

3.3.4 Setup and Equipment

Typically, large ovens are used for the annealing process. The inside of the oven is large enough to place the work piece in a position to receive maximum exposure to the circulating heated air. For high volume process annealing, gas fired conveyor furnaces are often used. For large work piece or high quantity parts, car-bottom furnaces will be used in order to move the parts in and out with ease. Once the annealing process has been successfully completed, the work pieces are sometimes left in the oven in order for the parts to have a controlled cooling process. While some work pieces are left in the oven to cool in a controlled fashion, other materials and

alloys are removed from the oven. After being removed from the oven, the work pieces are often quickly cooled off in a process known as quench hardening. Some typical methods of quench hardening materials involve the use of media such as air, water, oil or salt. Quench hardening is generally applicable for some ferrous alloys, but not copper alloys.

3.4 Thermal Treatment of the Nanocrystalline Amorphous Ribbon

With a view to study nanocrystallization behavior by XRD and magnetic properties upon evaluation of nanocrystalline phase on amorphous matrix, thermal treatment, i.e. annealing is required to perform. For XRD, as prepared amorphous ribbon were cut into small pieces of about 2cm lengths for annealing treatment. MTI Corporation built GSL-1600x40 tube furnace used for this purpose shown in Figure 3.9. The samples were put into the tube and filled up with Nitrogen gas before the tube furnace heated to a predefined temperature and kept for the time (30 minute) required completing the annealing. In this way all the isothermal annealing as a function of time were performed.

Figure 3.9 MTI - GSL-1600x40 Tube Furnaces

3.5 Powder/ Polycrystalline Diffraction

About 90% of all solid materials can be described as crystalline. When X-ray interacts with a crystalline substance (phase) one get a diffraction pattern. The X-ray diffraction pattern of a pure substance is, therefore, like a fingerprint of the substance. The powder diffraction method is thus ideally suited for characterization and identification of polycrystalline phases. Today about 50000 inorganic and 25000 organic single components, crystalline phase and diffraction patterns have been collected and stored on magnetic or optical media as standers. The main use of powder diffraction is to identify components in a sample by a search match procedure. Furthermore, the areas under the peak are related to the amount of each phase present in the sample.

3.5.1 Theoretical Considerations of X-ray Diffraction (XRD)

The German Physicist Wilhelm Roentgen discovered X-rays in 1895. X-rays are electromagnetic waves of short wavelengths in the range of 10^{-2} to 10^{2}Å. Unlike ordinary light, these rays are invisible, but they travel in straight lines and affect photographic film in the same way as light. On the other hand, they were much more penetrating than light and could easily pass through the human body, wood, quite thick pieces of metal and other "opaque" objects.

The XRD provides substantial of information on the crystal structure. XRD is one of the oldest and effective tools for the determination of the atomic arrangement in a crystal. The wavelength (1Å) of an X-ray is the same order of magnitude as the lattice constant of crystals and it is this which makes X-rays so useful in structural analysis of crystal. Whenever X-rays are incident on a crystal surface, they are reflected from it. The reflection abides by the Bragg's Law as given below

$$2d\sin\theta = n\lambda \qquad (3.2)$$

Where d is the distance between crystal plane, θ is the incident angle, λ is the wavelength of the X-ray and n is a positive integer. Bragg's Law also suggested that the diffraction is only possible when $\lambda < 2d$.

X-ray diffractograms of all the samples were recorded using monochromatic Cu-K_α radiation (λ = 1.54053 Å) to ensure the formation of single-phase nature of the product. XRD patterns information are: scanning speed 2°, chart speed 20 mm, starting from 30° and ending at 90°. Peak intensities are recorded corresponding to their 2θ values. The inter planner distance - d was calculated from these 2θ values of the diffraction peaks using the Bragg's Law (In Figure 3.10).

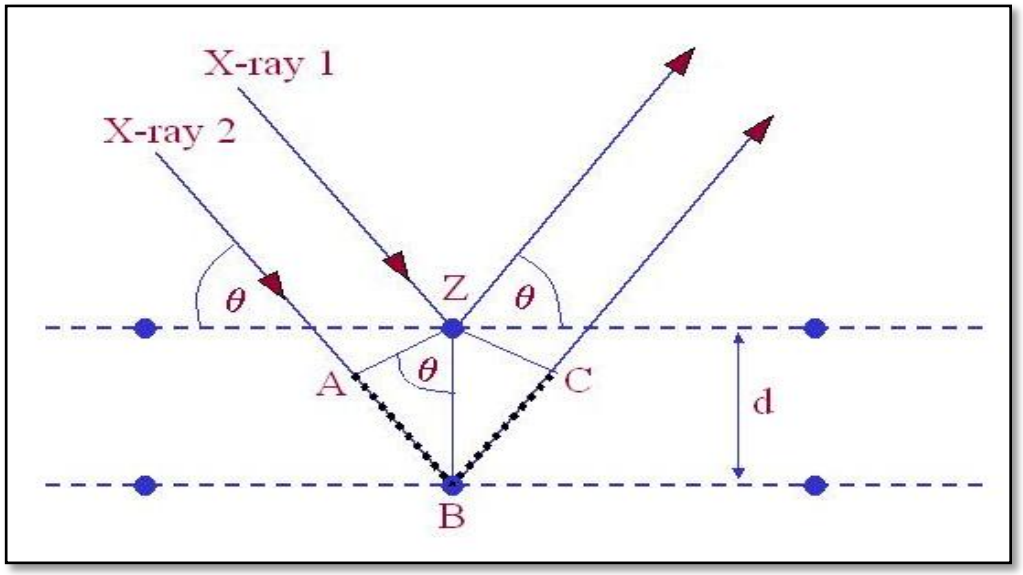

Figure 3.10 Bragg's diffraction pattern

Therefore the two possible values where we can have reflections are determined by the unit cell dimensions. However, the intensities of the reflection are determined by the distribution of the electrons in the unit cell. The highest electron density is found around atoms. Therefore, the intensities depend on what kind of atoms we have and where in the unit cell they are located. Planes going through areas with high electron density will reflect strongly, planes with low electron density will give weak intensities.

3.5.2 X-ray Powder Method

Powder method is perhaps the most widely used X-ray diffraction technique for characterizing materials. The term 'powder' really means that the crystalline domains are randomly oriented in the sample. Therefore, when the 2-D diffraction pattern is recorded, it shows concentric rings of scattering peaks corresponding to the various d spacing in the crystal lattice. The positions and the intensities of the peaks

are used for identifying the underlying structure (or phase) of the material. Powder diffraction data can be collected using either transmission or reflection geometry, as shown in Figure 3.11 below.

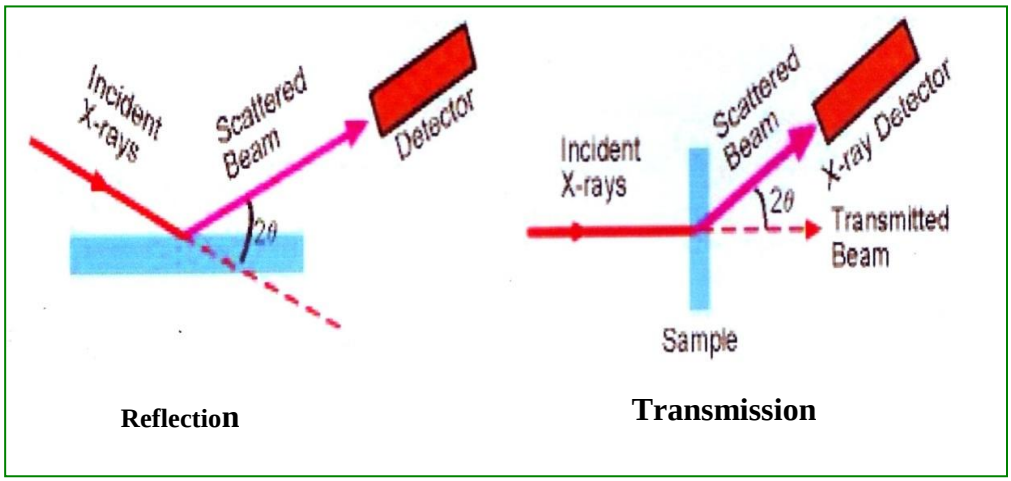

Figure 3.11 Reflection and Transmission geometry of powder diffraction

Because the particles in the powder sample are randomly oriented, these two methods will yield the same data. Powder diffraction data are measured using Bruker AXS D8 Advance diffractometer, which measures data in reflection mode and is used mostly with solid samples, or the custom built 4-circle diffractometer, which operates in transmission mode and is more suitable for liquid phase samples.

3.5.3 Experimental Technique for X-ray Diffractometer

X-ray diffraction (XRD) is a versatile non-destructive analytical technique for identification and quantitative determination of various crystalline phases of powdered or solid samples of any compound. For each set of composition, ribbons are cut into several pieces; each of length 20 mm. Heat treatment was performed on the amorphous ribbons using a tube furnace which filled by Nitrogen gas. After the heat treatment, samples were removed from the furnace tube carefully and kept separately for XRD experiment.

For XRD experiment each sample was set on a glass slides and fixed the sample by putting adhesive tape at the two ends of the sample. After the pattern is obtained the value of 2θ is calculated for each diffraction line; set of 2θ values is the raw data for the determination of the lattice parameters of the unit cell. Figure 3.12: Shows the block diagram of Bruker AXS D8 Advance X-ray diffractometer. The Bucker AXS D8 Advance X-ray diffractometer was used for the lattice parameter

determination in the PP&PDC, Materials Science Division, Bangladesh Council of Scientific and Industrial Research (BCSIR), Dhaka. Figure 3.13 shows the inside view of the Bucker AXS D8 Advance XRD system. The Bruker AXS D8 Advance diffraction system utilizes a modular system approach to provide performance for application ranging from routine characterization to in-depth research investigation.

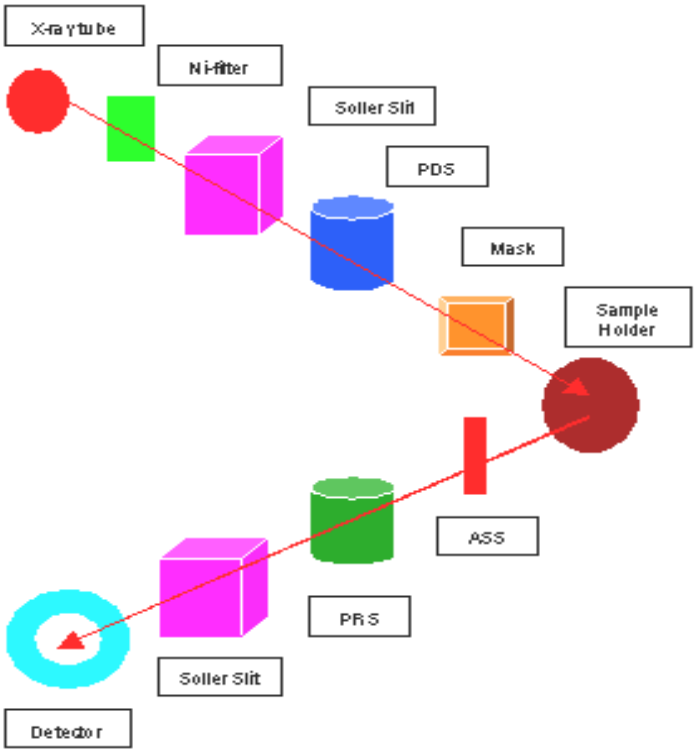

Figure 3.12 Block diagram of the Bruker AXS D8 Advance XRD system

The powder diffraction technique was used with a primary beam power of 40 kV and 40 mA for Cu radiation. A nickel filter was used to reduce Cu-K_α radiation and finally Cu-K_α radiation was only used as the primary beam. A (θ- 2θ) scan was taken from 30^o to 90^o to get possible fundamental peaks of the sample with the sampling pitch of 0.02^o and time for each step data collection was 1.0 sec. Both the programmable divergence and receiving slits were used to control the irradiated beam area and output intensity from the sample respectively.

An anti-scatter slit was used just after the sample holder to reduce air scattering. Two solar slits were used just after the tube and in front of the detector to get parallel beam only. All the data of the samples were stored in the computer memory and later analyzed that using computer software "DIFFRAC^{plus}".

Figure 3.13 Bruker AXS D8 Advance

The Bruker AXS D8 ADVANCE has the ability to perform a full range of applications, from qualitative and quantitative phase identification, under ambient or non-ambient conditions, to crystal structure solution from powder samples, crystallite size determination, micro strain analysis, residual stress analysis, and preferred orientation.

Bruker AXS D8 Advance SPECIFICATIONS	
X-RAY SOURCE	2.2kW Cu and Co, Running condition (40kV, 40mA), Power stability is better than 0.01%
DETECTORS	Point detector, Vantec-1 detector
OPTICS	Gobel Mirror
GONIOMETER	High precision microprocessor controlled, two circle goniometer with independent stepper motors and optical encoders; Smallest angular step 0.0001°; Reproducibility +/- 0.0001°
SAMPLE STAGE	Centric ¼-Circle Eulerian Cradle.Motorized Chi (tilt) and Phi (rotation) rotations and X-Y-Z translations. The cradle accommodates bulky specimens, powders, thin-films, and wafers up to 80 x 50 x 20 mm and weighing up to 1 kg
ATTACHEMENTS	High Temperature MRI stage (RT-1400C), Thin Film Reflectometry, sample spinner, video camera, sample plate with 9-sample holders
SOFTWARE	LEPTOZ, TOPAZ, ICCD

Attributes	
Depth	1135 mm
Height	1868 mm
Width	1300 mm
Weight	770 kg
Additional Specifications	Configurations: Vertical goniometer, Theta/2Theta or Theta/Theta geometry Measuring circle diameter: Predefined at 500 mm, 560 mm and 600 mm or any intermediate setting Angular range: 360° Max. usable angular range: –110° < 2Theta 168° Angle positioning: Stepper motors with optical encoders Smallest addressable increment: 0.0001° Instrument alignment: Equal or better than ± 0.01° 2Theta; NIST SRM 1976a always included Maximum angular speed: 20°/s Detectors: Point detectors: Scintillation counter SOL-XE energy dispersive 1-D detectors: LYNXEYE, VÅNTEC-1 All detectors guaranteed without defective/dead strips or areas Cooling water supply: Min. 4 l/min, pressure 4 bar to 7.5 bar, no pressure on outlet side, temperature: 10 °C to 20 °C Power supply: Single phase: 208 to 240 V, Three phases: 120 V, 230 V, 240V; 47 to 63 Hz

3.6 Analysis of XRD data

The XRD data consisting of $\theta_{hkl}$and d_{hkl} values corresponding to the different planes from which the following structural information of the nanocrystalline ribbon sample was evaluated.

(i) Identification of phases

(ii) Lattice parameter determination

(iii) Average grain size determination

(iv) Si- content determination in nanograins

(i) Identification of phases

The most common use of powder (polycrystalline) diffraction is chemical analysis. This can include phase identification (search/match), investigation of high/low temperature phase, solid solutions and determination of unit cell parameter of new materials.

XRD has become a very popular and useful instrument for routine X-ray analysis of nanocrystalline amorphous ribbon samples. In fact the diffractometer technique is often preferred to Debye-Scherrer technique owing to its several inherent merits. The most striking difference between the two methods is in the use of different intensity detection and measuring devices. XRD pattern of as-cast indicates just amorphous pattern of the given composition. The XRD patterns are identified as bcc α-Fe (Si) solid solution, which are developed on the nanocrystalline amorphous ribbon after heat treatment. The peak pattern is observed for all the samples at different heat treatment temperatures indicating the bcc α-Fe (Si) phase, which is developed on amorphous ribbons after heat treatment. Present experiment revels that 450°C is not sufficient temperature to start forming of crystalline nanograins of bcc Fe (Si) on the amorphous ribbon of the studied alloy composition.

(ii) Lattice Parameter Determination

Lattice parameter of crystalline bcc Fe-Si nanograin has been determined for all the two different amorphous compositions at different heat treatment temperatures. Normally, lattice parameter of an alloy composition is determined by the Debye-Scherrer method after extrapolation of the curve. In the present case, only one reflection (110) is prominent in all XRD patterns and we would like to understand how the value of lattice parameter changes with annealing temperature. We have, therefore, determined the lattice parameter using only that particular reflection using equation $2d\sin\theta = \lambda$ and $a_0 = d\sqrt{2}$, where $\lambda = 1.54178\,\text{Å}$ for $Cu - K_\alpha$ radiation and a_0 is the determined lattice parameter within an error estimated to be $\pm 0.0001\,\text{Å}$.

(iii) Grain Size Determination

The main aim (vital point) of the present study is to determine the nanocrystalline grain size for all the heat treated samples of the alloy composition by using Scherrer method. The XRD pattern of (110) reflection for different steps of heat treatment temperature of the alloy composition is used to calculate grain size. Grain size is determined using the following formula,

$$D_g = \frac{0.9\lambda}{\beta\cos\theta} \tag{3.3}$$

Where $\lambda = 1.54178\,\text{Å}$ for $Cu - K_\alpha$ radiation and β = FWHM (full width at half maximum) of the peak in radian. Considering β in degree we get the following relation

$$D_g = \frac{79.5}{\beta \cos\theta} \qquad (3.4)$$

All the values of grain size for every steps of heat treatment temperature of the alloy composition were determined. The FWHM of the peak is large at the early heat treatment temperature and with the increase of heat treatment temperature the value of FWHM becomes smaller which means that the grain size is increasing gradually.

(iv) Si-content in Nanograins

Crystalline nanograins were formed on the amorphous matrix of the ribbon in the process of heat treatment having the composition of Fe-Si. It is, therefore important to determine the concentration of Fe and Si in the nanograin [2.15]. As because the alloy consists of Fe and Si and we have experimentally determined the lattice parameter of the alloy nanograin for the two compositions at different temperatures. It is easy to calculate the Si content in the nanograins from the data of Pearsons who was established the relationship between the lattice parameter as dependent on Si content in Fe-Si alloys covering a wide range of composition [3.6]. From the relationship, we have constructed a simple equation to calculate Si content from lattice parameter. The equation is

$$X = \frac{(a_0 - 2.8812)}{0.0022} \qquad (3.5)$$

Where X is at. % Si in the nanograins, a_0 is the determined lattice parameter of nanograins. Si-contents for the nanograins develop during the isothermal annealing at various temperatures have been calculated.

3.7 Magnetization Measurement Techniques

In the present study magnetization has been performed using a Vibrating Sample Magnetometer (VSM).

3.7.1 Vibrating Sample Magnetometer (VSM)

A vibrating sample magnetometer (VSM) operates on Faraday's Law of Induction, which tells us that a changing magnetic field will produce an electric field. This electric field can be measured and can tell us information about the changing

magnetic field. A VSM is used to measure the magnetic behavior of magnetic materials. VSM is a versatile and sensitive method of measuring magnetic properties developed by S. Foner [3.7-3.8] and is based on the flux change in a coil when the sample is vibrated near it. The VSM is designed to continuously measure the magnetic properties of materials as a function of temperature and field. In this type of magnetometer, the sample is vibrated up and down in a region surrounded by several pickup coils. The magnetic sample is thus acting as a time-changing magnetic flux, varying inside a particular region of fixed area. From Maxwell's law it is known that a time varying magnetic flux is accompanied by an electric field and the field induces a voltage in pickup coils. This alternating voltage signal is processed by a control unit system, in order to increase the signal to noise ratio. The result is a measure of the magnetization of the sample.

3.7.2 Principle of VSM

The principle of VSM is as follows: when the sample of a magnetic material is placed in a uniform magnetic field, a dipole moment proportional to the product of the sample susceptibility times the applied field is induced in sample. If the sample is made to undergo a sinusoidal motion, an electrical signal is induced in suitably located stationary pick-up coils. This signal which is at the vibrating frequency, is proportional to the magnetic moment, vibration amplitude and vibration frequency. In order to obtain the reading of the moment only, a capacitor is made to generate another signal for comparison which varies in its moment, vibration amplitudes and vibration frequency in the same manner as does the signal from the pick-up coil. These two signals are applied to the two inputs of a differential amplifier, and because the differential amplifier passes only difference between the two signals, the effects of vibration amplitude and frequency changes are cancelled. Thus only the moment determines the amplitude of the signal at the output of the differential amplifier. This signal is in turns applied to a lock-in amplifier, where it is compared with the reference signal which is at its internal oscillator frequency and is also applied to transducer which oscillation the sample rod. Thus the output of the lock-in amplifier is proportional to the magnetic moment of the sample only avoiding any noise of frequency other that of the signal. The lock-in action yields an accuracy of 0.05% of full scale. The absolute accuracy of this system is better than 2% and reproducibility is better than 1%. Least measureable moment is $\mathbf{5 \times 10^{-4}}$ emu.

Figure 3.14 Vibrating Sample Magnetometer (VSM)

These measurements were carried out at Materials Science Division, Atomic Energy Center, Dhaka. We use Hirst VSM02 which is an automatic VSM for characterization of soft and hard magnetic materials manufactured by HIRST Magnetic Instruments Ltd. The Hirst VSM system arrangement is shown in the Figure 3.14.

RESULTS AND DISCUSSION

4.0 Results and Discussion

4.1 Differential Thermal Analysis Results

The understanding of the crystallization kinetics of magnetic amorphous alloys is of scientific interest as it represents a phase transformation occuring under extreme conditions far from equilibrium. Crystallization kinetics of magnetic material is often determined from Differential Scanning Calorimetry (DSC), Differential Thermal Analysis (DTA) and Thermomagnetic Analysis (TMA) [4.1-4.3]. The calorimetric studies of amorphous alloys provide substantial funfamental information concerning the kinetics of the crystallization have been studied calorimetrically by Clements and Cantor [4.4] and bothcalorimetrically and magnetically by Luborsky [4.5] in a variety of amorphous magnetic alloys. If the amorphous alloy is to be used as a precursor for the production of nanocrystalline FINEMET of composition Fe-Cu-Nb-B-Si then the primary and secondary crystallization temperatures are of importance. Because the structure of the benificial ferromagnetic nanocrystalline phase is composed of $\alpha - Fe(Si)$ which is the product of primary crystallization. The secondary crystallization product is the Fe_2B phase. This boride phase is detrimental for the soft magnetic properties because of its high anisotripy. In the present investigation DTA technique has been used to study the crystalline behavior of nanocrystalline alloy with composition $Fe_{72.5}Cr_1Nb_3Cu_1Si_{13.5}B_9$. DTA data are then analyzed within frame work of kinetic rate law and activation energy for corresponding crystallization peak extracted. Crystallization have also beenstudied by a sign X-ray diffraction (XRD). The X-ray diffraction experiment was undergone to identify the revolution of phases with heat treatment.

4.1.1 DTA Results of Nanocrystalline Amorphous Ribbon with Composition $Fe_{72.5}Cr_1Nb_3Cu_1Si_{13.5}B_9$

DTA traces of as-cast nanocrystalline amorphous ribbon $Fe_{72.5}Cr_1Nb_3Cu_1Si_{13.5}B_9$ alloy taken in nitrogen atmosphere with the heating rates of 10^oC – 60^oC/minute at the step of 10^oC with continuous heating from room temperature to 800^oC, are presented in Figure 4.1 (a) to Figure 4.1 (f), respectively. In each of the figure, two exothermic peaks are distinctly observed which corresponds to

two different crystallization events at temperature T_{x_1} and T_{x_2}, respectively. The soft magnetic ribbon corresponds to close in which primary crystallization (T_{x_1}) of α-Fe(Si) takes place. Secondary crystallization (T_{x_2}) of Fe_2B caused magnetic hardening of the nanocrystalline alloy. Mechanical hardening of the amorphous precursor has been observed in incipient primary crystallization and attributed to Cu nucleation. Phase identification cannot be done from a DTA scan. XRD has been used for the identification of phases and would be discussed later on. Thus, the identification of these two temperature, is necessary to understand the appropriate temperature range for heat treatment in order to achieve the nanocrystalline phase and thereby, suitable range of temperature for application of alloy. DTA is a direct and effective way to analyze the kinetics of nanocrystalline materials in respect of phase transition. The change of composition affects atomic ordering through nucleation and growth of crystallites. Again, the composition of alloy affects both the primary and secondary crystallized phases, because the time needed for constituent atoms to arrange themselves in a long range order depends on their bond energies [4.6].

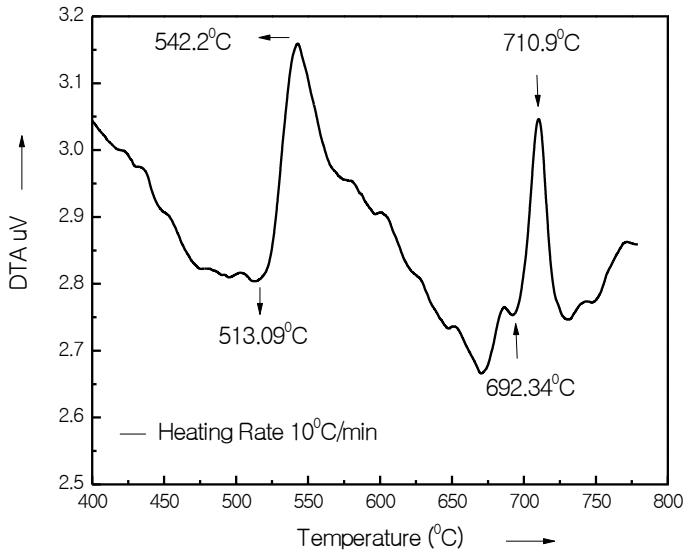

Figure 4.1 (a) DTA trace of as-cast nanocrystalline amorphous ribbon $Fe_{72.5}Cr_1Nb_3Cu_1Si_{13.5}B_9$ at the heating rate of 10^oC/min

DTA trace of as cast nanocrystalline amorphous ribbon sample recorded in a nitrogen atmosphere with a heating rate 10^oC/min has been represented in Figure 4.1 (a). Two exothermic peaks are observed which corresponds to two different

crystallization events at temperature 542.2^{o}C and 710.9^{o}C, respectively. Both anomalies are followed by sharp peaks, which corresponds to the release of heat of these temperatures due to change in the ordering of the atoms.

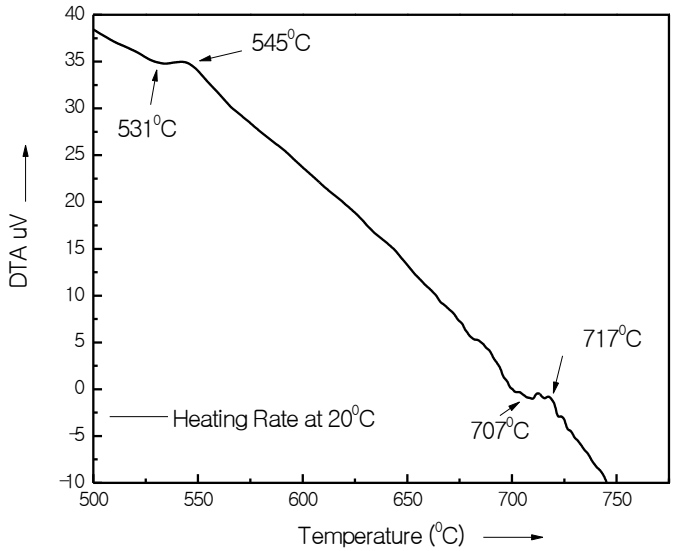

Figure 4.1 (b) DTA trace of as-cast nanocrystalline amorphous ribbon $Fe_{72.5}Cr_1Nb_3Cu_1Si_{13.5}B_9$ at the heating rate of 20^{o}C/min

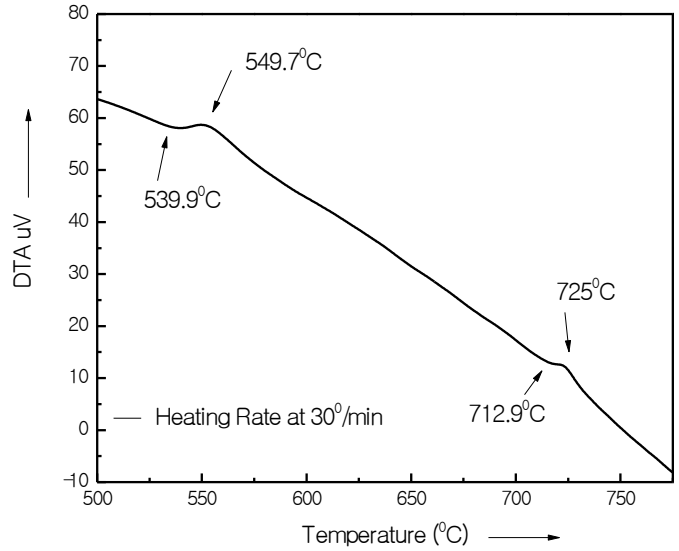

Figure 4.1 (c) DTA trace of as-cast nanocrystalline amorphous ribbon $Fe_{72.5}Cr_1Nb_3Cu_1Si_{13.5}B_9$ at the heating rate of 30^{o}C/min

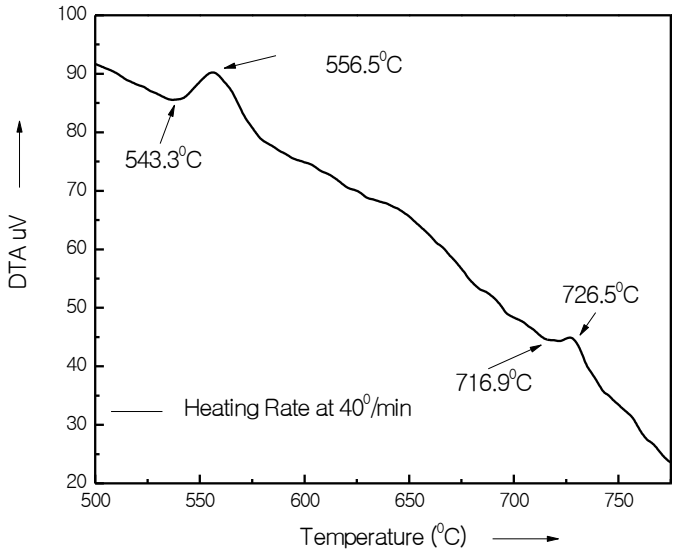

Figure 4.1 (d) DTA trace of as-cast nanocrystalline amorphous ribbon $Fe_{72.5}Cr_1Nb_3Cu_1Si_{13.5}B_9$ at the heating rate of 40°C/min

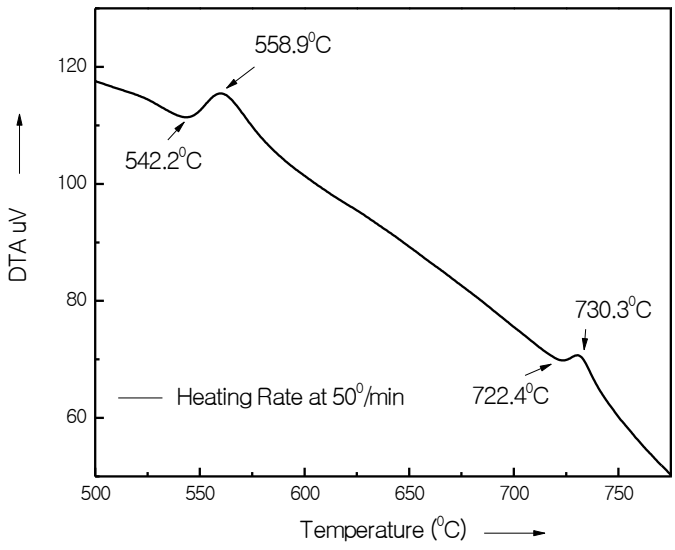

Figure 4.1 (e) DTA trace of as-cast nanocrystalline amorphous ribbon $Fe_{72.5}Cr_1Nb_3Cu_1Si_{13.5}B_9$ at the heating rate of 50°C/min

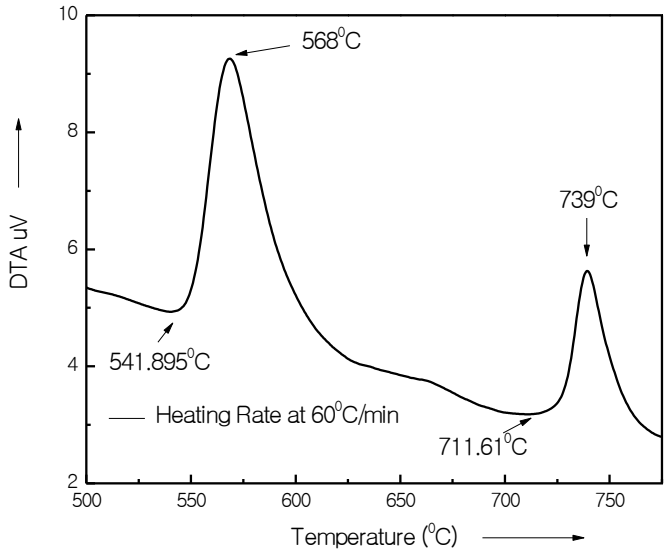

Figure 4.1 (f) DTA trace of as-cast nanocrystalline amorphous ribbon $Fe_{72.5}Cr_1Nb_3Cu_1Si_{13.5}B_9$ at the heating rate of 60°C/min

Figure 4.1(a) to Figure 4.1 (f) shows DTA traces and is observed that the crystallization of each phase has occurred over a wide range temperatures and that the peak temperatures shift to higher values with the increase of heating rate. That means, it required more heat energy for the formation of crystalline phases with increasing heating rates. The crystallization of each phase occurs over a wide range of temperature.

From each of the DTA traces, it is obvious that the area under the first crystallization peak is larger than the area covered by the second crystallization peak. In the Table 4.1 crystallization peak temperatures of two phases (T_{p_1} and T_{p_2}) and crystallization onset temperatures of two phases ($T_{x_1}$and T_{x_2}) are given for different heating rates.

It has been observed that the crystallization temperature range of first phase occurred within 9.8°C to 29.11°C but this range for the second crystallization phase is 7.9°C to 27.39°C. So it is notable that the crystallization temperature range for first peak is always larger than the second peak. It is also observed that the peak temperature shift to higher values and crystallization temperature range increase with the heating rates.

Table 4.1 Effect of heating rate on 1st and 2nd crystallization states of the nanocrystalline amorphous ribbon with composition $Fe_{72.5}Cr_1Nb_3Cu_1Si_{13.5}B_9$

Heating rate β^0C/min	1st starting $T_{x1}{}^0$C	1st Peak $T_{p1}{}^o$C	Temperature range of 1st state in ^{0}C	2nd starting $T_{x2}{}^o$C	2nd Peak $T_{p2}{}^o$C	Temperature range of 2nd state in ^{0}C	T_{x2} - T_{x1} in ^{0}C	T_{p2} - T_{p1} in ^{0}C
10	513.09	542.2	29.11	692.3	710.9	18	179.21	168.7
20	531	545	14	707	717	10	176	172
30	539.9	549.7	9.8	712.9	725.5	12.1	173	175.3
40	543.3	556.5	13.2	716.9	726.5	9.6	173.6	170
50	542.2	558.9	16.7	722.4	730.3	7.9	180.2	171.4
60	541.9	568	26.11	711.61	739	27.39	169.7	171

From table 4.1 are seen that starting crystallization temperature gap $[T_{x_2} - T_{x_1}]$ and two crystallization peak gap $[T_{p_2} - T_{p_1}]$ phenomena has taken place within a large temperature gap of around 169.7^{o}C to 180.2^{o}C and 168.7^{o}C to 175.3^{o}C, respectively. There is difference of 175 ± 5^{o}C for the two crystallization temperature. This implies that Cr-content alloys weaken the diffusion process to form the crystallization phases since has a melting temperature (1857^{o}C) higher than that of Fe(1536^{o}C). From our experimental finding it is clearly understood that the partial substitution of Fe by Cr enhance thermal stability of amorphous alloys against crystallization.

The activation energy of crystallization of $T_{x_1}$and T_{x_2} phases have been calculated using Kissinger equation [4.7].

$$\beta = T_p^2 e^{-E/KT_p}$$

$$\ln(\frac{\beta}{T_p^2}) = -\frac{E}{KT_p}$$

$$E = -KT_p \ln(\frac{\beta}{T_p^2}) \qquad (4.1)$$

Where β is the heating rate, T_p is the crystallization temperature, E is the activation energy and K is the Boltzmann constant. The activation energy of T_{x_1}[α-Fe(Si)] and T_{x_2}[Fe_2B] phases has been calculated from Table 4.2 and using Kissinger's plot shown in Figure 4.2 (a) and Figure 4.2 (b). It shows that first thermal crystallization activation energy of α-Fe(Si) phase E_1 is 3.26 eV and second Fe_2B phase E_2 is 4.871 eV. The activation energy for formation of the first crystalline $\alpha - Fe(Si)$ phase is small higher than that for the original FINEMET [4.8] composition which is expected

due to replacement of Fe by Cr. As depicted above, the apparent activation energy E_c and E_g respectively. At this stage, formation of Cu clusters leads to a small higher activation energy for preferential nucleation. However, with the decrease of crystalline volume fraction, the Cu-rich regions gradually run out.

Table 4.2 Effect of heating rate on 1st and 2nd crystallization of the nanocrystalline amorphous ribbon with composition $Fe_{72.5}Cr_1Nb_3Cu_1Si_{13.5}B_9$ state's calculative data for activation energy calculation data

Heating rate β^0C/min	Heating rate β^0K/min	1st Peak $T_{p1}{}^oK$	$1/T_{p1}$ x 10^3	ln $(\beta/T_{p1}{}^2)$	2nd Peak $T_{p2}{}^oK$	$1/T_{p2}$ x 10^3	ln $(\beta/T_{p2}{}^2)$
10	13.41	815.2	1.23	-10.81	983.9	1.02	-11.19
20	26.89	818	1.22	-10.12	990	1.01	-10.5
30	40.24	822.7	1.22	-9.73	998.5	1.00	-10.11
40	53.66	829.5	1.21	-9.46	999.5	1.00	-9.83
50	67.07	831.9	1.20	-9.24	1003.3	0.997	-9.62
60	80.46	841.9	1.1878	-9.08	1012	0.988	-9.45

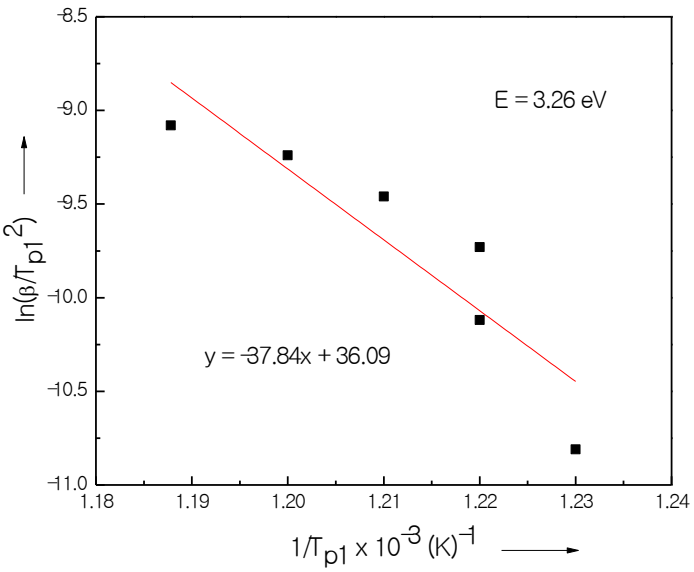

Figure 4.2 (a) Kissinger's plot to determine the activation of Fe (Si) phase for $Fe_{72.5}Cr_1Nb_3Cu_1Si_{13.5}B_9$ alloy

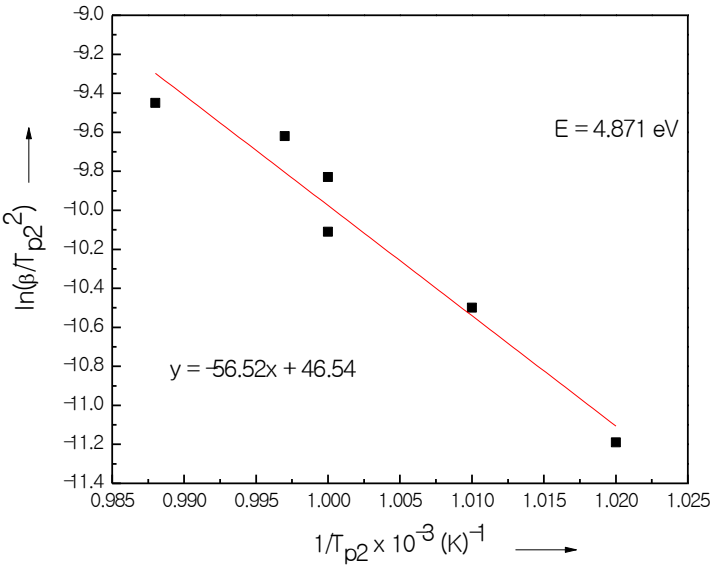

Figure 4.2 (b) Kissinger's plot to determine the activation of Fe_2B phase for $Fe_{72.5}Cr_1Nb_3Cu_1Si_{13.5}B_9$ alloy

4.1.2 Annealing effects on the kinetics of structural relaxation of $Fe_{72.5}Cr_1Nb_3Cu_1Si_{13.5}B_9$ nanocrystalline amorphous ribbon studied by DTA

The experimental data have been interpreted in terms of different annealing effects on amorphous ribbon of DTA traces at constant heating rate 20°C/min. The DTA traces of $Fe_{72.5}Cr_1Nb_3Cu_1Si_{13.5}B_9$ alloy in the as cast state and annealed at different temperatures for 30 min are shown in Figure 4.3 (a) to 4.3 (d) respectively. Effect of annealing at different temperatures of the amorphous ribbons on their crystallization behavior by DTA scan have been performed on both the samples with continuous heating at 20°C/min heating rate.

It is observed from the DTA scan that the onset temperature for the sample $Fe_{72.5}Cr_1Nb_3Cu_1Si_{13.5}B_9$ annealed at T = 450°C is almost unchanged with respect to its amorphous precursor which is quite logical since T = 450°C is still lower than its T_{x_1} = 531°C. But the same sample when annealed at T = 550°C and 600°C which are higher than the onset of crystallization temperature of T_{x_1} = 531°C, the primary crystallization peak has completely diminished and display diffused character meaning that substantial amount of primary crystallization, $\alpha - Fe(Si)$ phase has already been completed for 30 minutes at T = 550°C and T = 600°C.

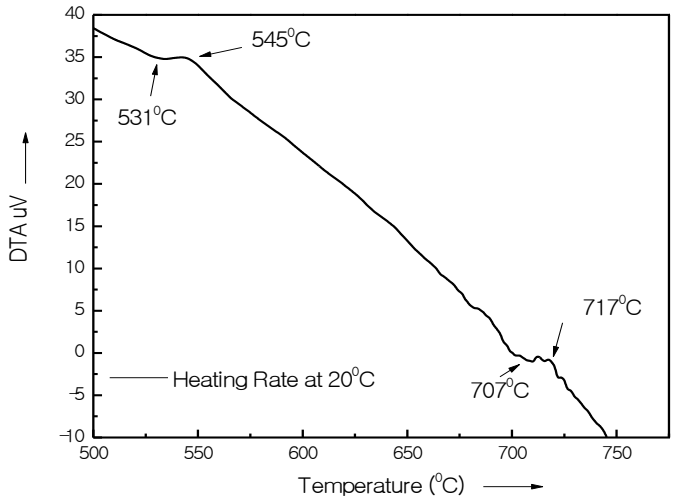

Figure 4.3 (a) DTA trace of as-cast nanocrystalline amorphous ribbon $Fe_{72.5}Cr_1Nb_3Cu_1Si_{13.5}B_9$ at the heating rate of 20°C/min

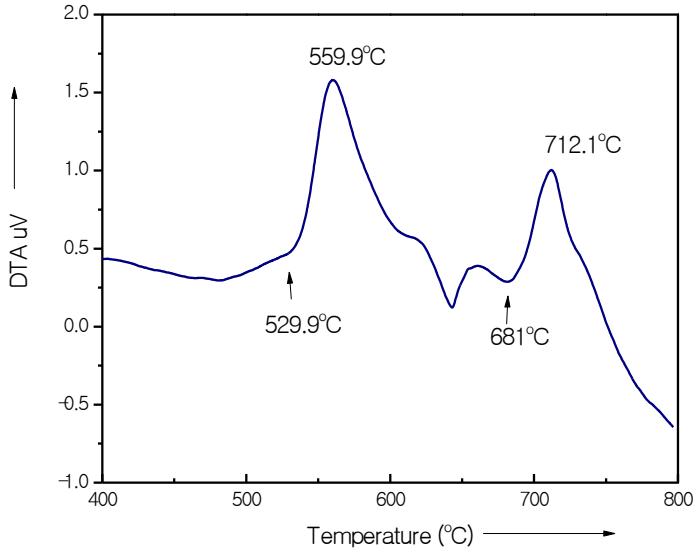

Figure 4.3 (b) Effects on DTA trace of annealing temperature 450°C on the nanocrystalline amorphous ribbon with composition $Fe_{72.5}Cr_1Nb_3Cu_1Si_{13.5}B_9$ at the heating rate of 20°C/min

The area under the first peak of DTA curve corresponds to the crystallization enthalpy, ΔH of $\alpha - Fe(Si)$ from which the volume fraction of crystallization (X_f) can be estimated according to the formula,

$$X_f = \frac{\Delta H_a - \Delta H_t}{\Delta H_a} \qquad (4.2)$$

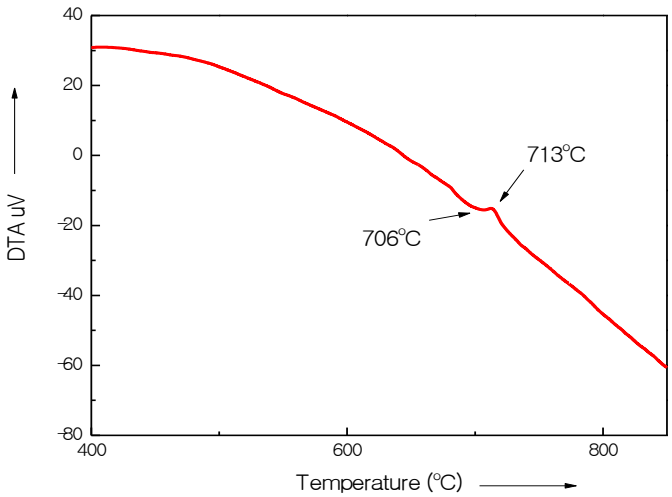

Figure 4.3 (c) Effects on DTA trace of annealing temperature 550°C on the nanocrystalline amorphous ribbon with composition $Fe_{72.5}Cr_1Nb_3Cu_1Si_{13.5}B_9$ at the heating rate of 20°C/min

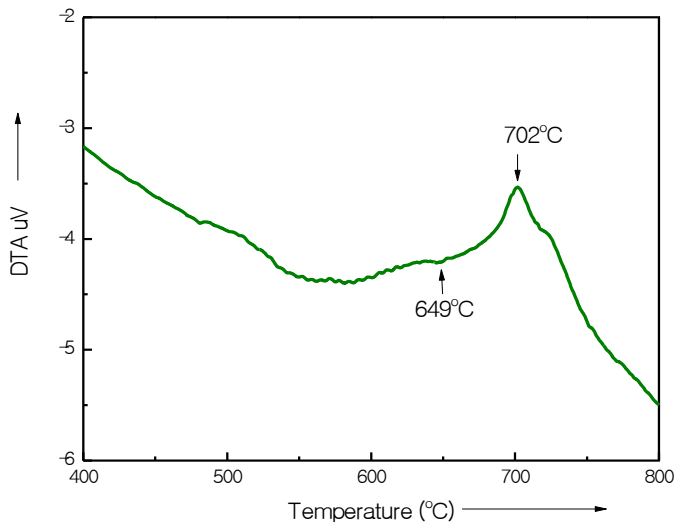

Figure 4.3 (d) Effects on DTA trace of annealing temperature 600°C on the nanocrystalline amorphous ribbon with composition $Fe_{72.5}Cr_1Nb_3Cu_1Si_{13.5}B_9$ at the heating rate of 20°C/min

where, ΔH_a and ΔH_t are the crystallization enthalpy of the as-cast alloy and that of the alloy annealed for a time t, respectively. This shows that with increasing annealing temperature X_f is expected to increase. The effect of annealing temperature T on the secondary crystallization is insignificant since the T is very low compared to T_{x_2} .The results of DTA scan on annealing of the sample with as-cast sample with the

parameter such as T_{x_1}, T_{x_2}, T_{p_1}, T_{p_2} and ΔT are depicted in Table 4.3. As cast and annealed samples at T_a = 450°C do not show any significant changes area under the first peak corresponding to the crystallization enthalpy, ΔH of $\alpha - Fe(Si)$. This means that at T_a = 450°C, no crystallization occurred which is quite obvious since T_{x_1} = 531°C for this sample. This demonstrates that even annealing at T_a = 450°C, the material still remained amorphous.

Therefore crystallization enthalpy ΔH (area under the peak) is almost equal that of, it's amorphous state. But when annealed at T_a = 550°C and T_a = 600°C, there are broad diffused first peak meaning that substantial amount of primary crystallization, $\alpha - Fe(Si)$ has already been completed for 30 minutes at T_a = 531°C. for T_a = 550°C and T_a = 600°C first DTA peak is almost not visible; i.e. $\alpha - Fe(Si)$ phase has almost completed. A critical scrutiny of 2nd peak does not show any significant changes are shown in Figure 4.3(c) and Figure 4.3 (d).

Table-4.3: Annealing effects on 1st and 2nd crystallization states of the nanocrystalline amorphous ribbon with composition $Fe_{72.5}Cr_1Nb_3Cu_1Si_{13.5}B_9$ at constant heating rate 20°C/min

Annealing Temperature	Onset Temp. of primary crystallization T_{x_1} °C	Primary crys. peak Temperature T_{p_1} °C	Onset Temp. of secondary crystallization T_{x_2} °C	Secondary crys. peak Temperature T_{p_2} °C	(ΔT) $T_{p_2} - T_{p_1}$ in °C
As-cast	531	545	707	717	172
450°C	529.9	559.9	681	712.1	152.2
550°C	_	_	706	713	_
600°C	_	_	649	702	_

It is observed from the table that the T_{x_1}, T_{x_2}, T_{p_1}, T_{p_2} as well as the difference between the two crystallization events are almost not affected by annealing, just

below the crystallization temperatures. When the samples are annealed above the T_{p_1}, the primary crystallization as evidenced from their DTA curves are so diffused and smeared that they give signals of nearly completion of the primary crystallization of $\alpha - Fe(Si)$ crystallites. Therefore no characteristic temperatures in this range could be determined.

4.2 Microstructural Analysis of Amorphous and Nanocrystalline $Fe_{72.5}Cr_1Nb_3Cu_1Si_{13.5}B_9$ Alloy by XRD Analysis

XRD experiment has been carried out in order to understand the evolution of microstructure with respect to different annealing temperature for 30 minutes. XRD has been used to identify crystalline phase in nanocrystalline alloy. In the present work, in order to study the crystallization onset temperature, XRD spectra have been recorded for the nominal composition $Fe_{72.5}Cr_1Nb_3Cu_1Si_{13.5}B_9$ annealed at 450^{o} to 800^{o} for 30 minutes. The approximately annealed samples were subjected to XRD by using a MTI Corporation built GSL-1600x40 tube furnace to examine the micro structural evaluation as a function of annealing temperature. From these experiment, obtained results of three kinds of structural parameter including lattice parameter, grain size and silicon content of nanocrystalline $\alpha - Fe(Si)$ grains from which are further attempt to find out the intrinsic and extrinsic magnetic properties.

Lattice Parameter of crystalline bcc Fe-Si nanograin was determined at different annealing temperature of the experimental alloys. Structure of the α-Fe(Si) grains depends on the annealing temperature. Generally for an accurate determination of the lattice parameter a number of fundamental peaks are required but in this type of tailored materials upon crystallization only major fundamental peaks (110) is used in calculation of a_o. We have, therefore, determined the lattice parameter using only that particular reflection using equation:

$$2d\sin\theta = n\lambda \text{ and } a_o = d\sqrt{2} \qquad (4.3)$$

Where λ = 1.54053 Å is the wavelength of Cu-K_α radiation and a_o is determined lattice parameter of the grain, d is the inter-planar spacing and θ is the diffraction angle. While grain size have been calculated using equation (3.3). One of the most important aims of this study was to determine crystalline grain size for all the annealing temperatures. Grain size of all annealed samples of the alloy composition was determined using Scherrer method [4.8].

Silicon content of the $\alpha - Fe(Si)$ nanograins was calculated from the established quantitative relationship between lattice parameter and Si-content in Fe-Si alloys by Bozorth [4.9 new]. All the results of θ, d values, full with at half maximum (FWHM) of the intensity peak corresponding to (110) planes, Grain size (D_g) and Si-content from XRD analysis are listed in Table-4.4

It is easy to calculate the Si content in the nanograin from the Pearson hand book relationship [4.9]. From this relationship we have considered a simple equation to calculate Si-content from lattice parameter. This equation is

$$b = -467a_o + 1342.8 \qquad (4.4)$$

Where b is at. % Si in the nanograins, a_o is the lattice parameter of nanograins.

4.2.1 Identification of Phases by XRD Experiment

The XRD patterns for the alloy $Fe_{72.5}Cr_1Nb_3Cu_1Si_{13.5}B_9$ annealed at temperature 450°C, 500°C, 550°C, 600°C, 650°C, 700°C, 750°C and 800°C each for 30 minutes presented in Figure 4.4. It is evident from Figure 4.4 when the sample annealed below 500°C, i.e. at 450 °C, it exhibited only one broad peak around 2θ = 45°C at the position of d_{110} reflection which is generally known as diffuse hallow. This diffuse hallow indicates the amorphous nature of the sample. It means at the annealing temperature below 500°C, no crystallization peak has been detected. So the onset crystallization temperature determined from these results is 500°C. The value of FWHM of the peak at the annealing temperature 550 °C is 0.865. For the higher annealing temperatures, the FWHM value is getting smaller. It shows that the crystallization occurs to a good extent at the higher annealing temperature. The crystallization onset temperatures from DTA experiment for different heating rates were found in the range of 513°C, which shows a good consistency with the XRD results.

For annealing at higher temperature i.e. 500 °C, 550 °C, 600 °C, 650 °C, 700 °C, 750 °C and 800 °C the $\alpha - Fe(Si)$ phases were found at the lower values of 2θ at 45.20°, 44.88°, 45.04°, 45.40°, 44.94° and 45.16° respectively with 100% peak intensity on (110) line. Other two fundamental peaks corresponding to $\alpha - Fe(Si)$ on (200) and (211) diffraction lines for annealing temperature at and above 500°C is obtained in this Figure 4.4. But due to their low intensity they are not clearly visible.

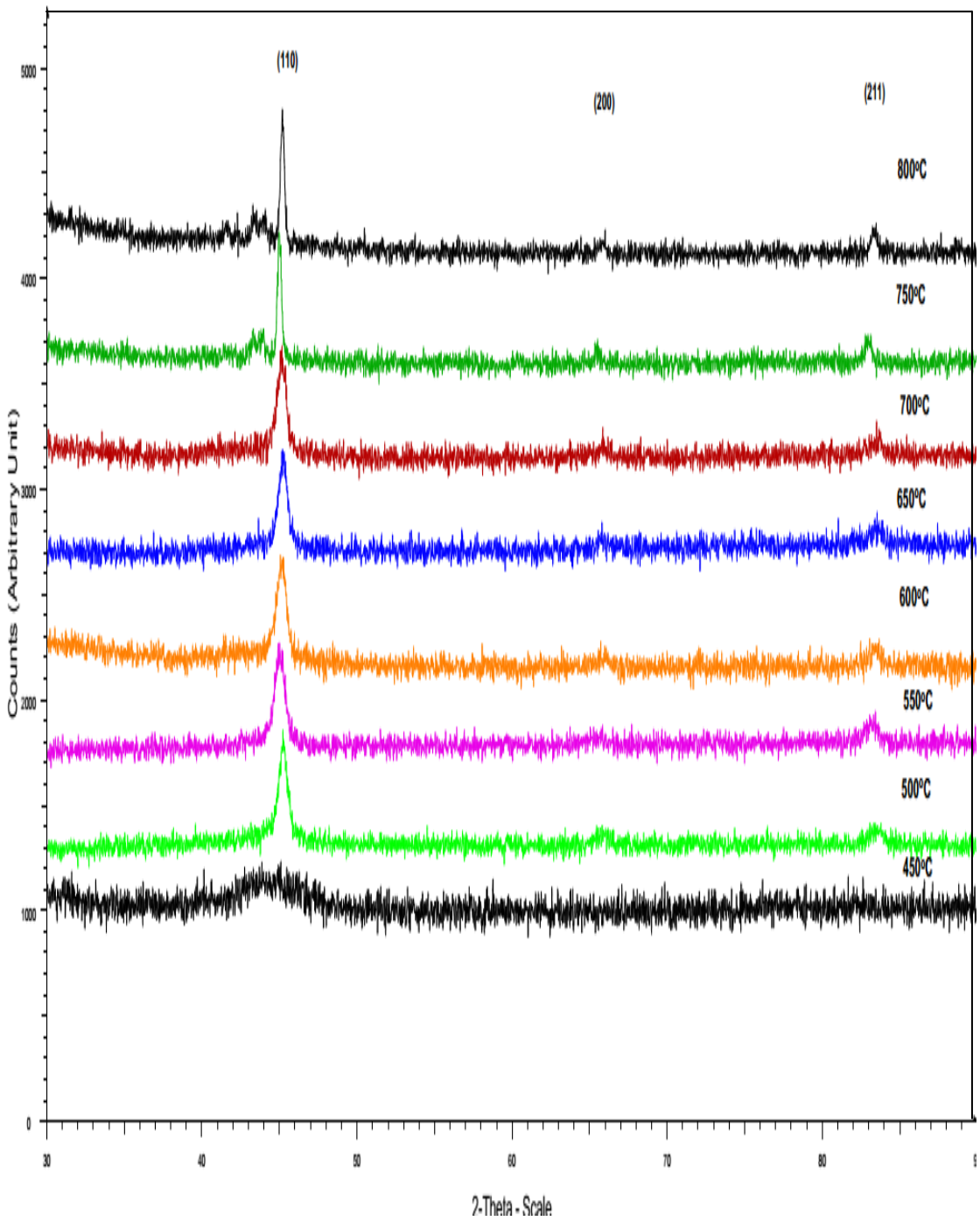

Figure 4.4 XRD spectra of $Fe_{72.5}Cr_1Nb_3Cu_1Si_{13.5}B_9$ alloys of annealed at different temperatures at constant annealing time 30 min

From DTA result it is expected that $\alpha - Fe(Si)$ phase would form beyond 550°C. The XRD pattern illustrated in Figure 4.4 reveal that the difference in Bragg's peak as well as the intensity of the fundamental reflection becomes gradually stronger

as the temperature of the heat treatment increases. This increase in the sharpness of the intensity peaks with the annealing temperature indicates that crystalline volume fraction has been increased and also grains become coarser with increased crystallinity. The systematic but negligible shift of peak towards the larger angles with increasing temperature indicates that lattice parameter of the phase gradually decreases due to the increasing of Si-content of $\alpha - Fe(Si)$ phase.

Table 4.4 Experimental XRD data of nanocrystalline $Fe_{72.5}Cr_1Nb_3Cu_1Si_{13.5}B_9$ amorphous ribbon at different annealing temperatures

Annealing Temp. in ^oC	θ (deg.)	d (Å)	FWHM (deg.)	a_0 (Å)	D_g (nm)	Si (at. %)
450	--	--	--	--	--	--
500	22.60	2.006	0.549	2.8369	16	18.25
550	22.44	2.0195	0.865	2.8560	10	9.05
600	22.52	2.012	0.72	2.8454	12	13.998
650	22.70	1.997	0.69	2.8242	12	23.9
700	22.57	2.009	0.60653	2.8412	14	15.96
750	22.47	2.012	0.317	2.8454	27	13.998
800	22.58	2.008	0.2888	2.8397	30	16.66

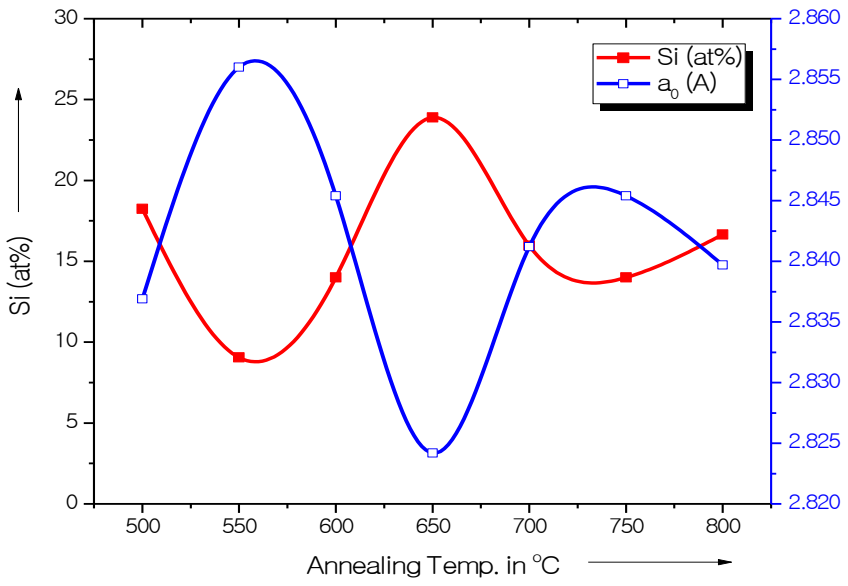

Figure 4.5 Change of Si (at. %) content and Lattice Parameter with different annealing temperature for the sample with composition $Fe_{72.5}Cr_1Nb_3Cu_1Si_{13.5}B_9$

The lattice parameter, the silicon content in bcc nanograins and grain size of $\alpha - Fe(Si)$ grain can easily be calculated from the fundamental peak of (110) reflections. All results are shown in Table 4.4.

4.2.2 Lattice Parameter Determination

Lattice parameter of crystalline $\alpha - Fe(Si)$ was determined at different annealing temperatures of the experimental alloys. Structure of the $\alpha - Fe(Si)$ grains depends on the annealing temperature. Figure 4.5 shows that, with the increase in annealing temperature lattice parameter increasing up to 550^{o}C, above the annealing temperature decreases. The lattice parameter of pure Fe is 2.8664Å. But the lattice parameter at various annealing temperature for the present alloy are significantly less than that of pure Fe. The percentage of partitioned Si in the nanocrystalline $\alpha - Fe(Si)$ phase is maximum at 650^{o}C. After 650^{o}C, decrease in Si-content is observed up to 750^{o}C, explained by the fact that at higher temperatures silicon diffuses out of nanograins due to crystallization corresponding to formation of boride phase which is consistent with the result of other FINEMET's. Si having a smaller atomic size compared to Fe, diffuses in the $\alpha - Fe(Si)$ lattice during annealing at different temperatures which results in a contraction of $\alpha - Fe(Si)$ lattice. So the more diffusion of Si, there should be more contraction of the $\alpha - Fe(Si)$ lattice and thereby, the decrease or increase of parameter.

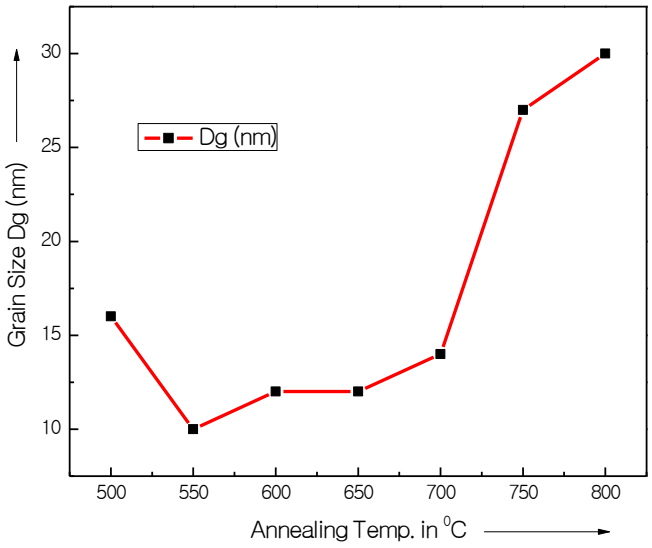

Figure 4.6 Change of Grain Size with different annealing temperature for the sample with composition $Fe_{72.5}Cr_1Nb_3Cu_1Si_{13.5}B_9$

However the decrease in lattice parameter is evident at or around 650^{o}C when the diffusion of Si became easier at that temperature due to stress-relief in microstructure caused by heat treatment. Figure 4.5 presents the inverse relationship between lattice parameter and Silicon content. When the sample up to 650^{o}C, the increase of Si-content with subsequent decrease of lattice parameter, as showed in Figure 4.5 indicates that silicon diffuse out of $\alpha - Fe(Si)$ grains for which the size of $\alpha - Fe$ lattice is regained.

4.2.3 Silicon Content in Nanograins

Lattice parameter measurements give the hint about a non-negligible solute content establishing the fact that the bcc-ferro-magnetic phase consists of Fe, Cr and Si essentially. The Si contents of the alloy $Fe_{72.5}Cr_1Nb_3Cu_1Si_{13.5}B_9$ at different annealing temperature 500^{o}C to 800^{o}C for 30 minutes are found to be in the range of 9.05% to 18.25%. All these results are presented in Table 4.4 and the pattern of change in Si-content with respect to annealing temperature is represented in Figure 4.5. Figure 4.5 represents the inverse relationship between lattice parameter and Si-content. This kind of relation between lattice parameter and Si-content was observed in the reports [4.10], which are verified in present work effectively. At the initial stage of crystallization lattice parameter first decreases with increase of Si-content, because Si diffuses in the bcc $\alpha - Fe$ phase, to form the soft nanocrystalline $\alpha - Fe$(Si) phase.

4.2.4 Grain Size Determination

In 1963 Kneller et.al. [4.11] studied on nanometric grains. They found that the magnetic properties of isolated grains change drastically as their size is reduced to the nanometer range. When these nanometric grains are consolidated to form a nanostructured material, the magnetic properties are largely determined by the grain size and the exchange interaction between the adjacent grains. Grain size of all annealed samples of the alloy composiotion was determined using Sherrer method [4.12]. Grain size was determined using equation (3.3). From Figure 4.4 it is clear that at lower annealing temperature 550^{o}C, the FWHM of the peak is large and with the increase of annealing temperature, the value of FWHM are getting smaller. The peaks are, therefore becoming sharper with the shifting of peak position towards higher 2θ

value. The peak shifts indicate the change of the values of Si content of the nanograins and therefore, the change of values of lattice parameter of nanograins.

Figure 4.4 and Table 4.4 shown at 450^{o}C, no evidence of Si partitioning was found at the annealing temperature and hence grain growth is still not so evident. The increase of annealing temperature initiates partitioning $\alpha - Fe$(Si) phase and thus grain growth due to formation of nanocrystalline $\alpha - Fe$(Si) grains. In the range of annealing temperature 500^{o}C to 800^{o}C, the grain size remains in the range of 10 to 30 nm corresponding to soft magnetic $\alpha - Fe$(Si) phases. Above 700^{o}C grain grow rapidly and attain maximum value 30 nm at 800^{o}C indicating formation of Fe_2B phases. Formation of boride phase is detrimental to soft magnetic properties as showed in further experimental and also supported by different reports [4.13]. These facts reveal that heat treatment temperature should be limited within 550^{o}C to 700^{o}C to obtain optimum soft magnetic behavior, which will be clear that nearly same grain size.

4.3 Magnetic Field Dependence of Magnetization

The magnetization of $Fe_{72.5}Cr_1Nb_3Cu_1Si_{13.5}B_9$ ribbon is measured as a function of magnetic field using vibrating sample magnetometer (VSM) [4.15]. In this type of magnetometer the sample is vibrated up and down in a region surrounded by several pick up coils. The magnetic sample is thus acting as a time changing magnetic flux; varying inside a particular region of fixed area. The lock-in-action of VSM yields an accuracy of 0.05% of the full scale. The absolute accuracy of this system is better than 2% and the reproducibility is better than 1%. Least measurable moment is 5x10^{-4}emu. The magnetometer was calibrated using a high purity-Ni disk. Considering the saturation magnetization of Ni is 54.75emu/gm at room temperature. The ribbon samples were cut into small shapes, weighed and glued to a standard sample holder.

The magnetization process of the nanocrystalline amorphous ribbon with different field are shown in Figure 4.7 from the magnetization curve it is clearly evidenced that the magnetization is saturated sample in amorphous state within an applied field of 500 Oe. Saturation magnetization (M_s) has been observed 122.6 emu/gm. Saturation magnetization value of M_s =160 emu/gm at room temperature for original FINEMET which decreases with the substitution of Fe magnetic moment by the substitution of non-magnetic Cr.

.

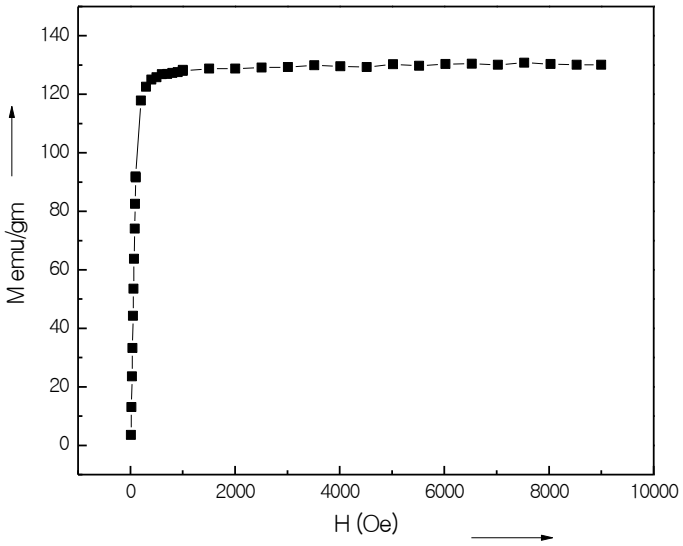

Figure 4.7 Magnetization versus magnetic field curves for the alloy with composition $Fe_{72.5}Cr_1Nb_3Cu_1Si_{13.5}B_9$

4.3.1 Temperature Dependence of Specific Magnetization $Fe_{72.5}Cr_1Nb_3Cu_1Si_{13.5}B_9$ Nanocrystalline Amorphous Ribbons

The variation of saturation magnetization (M_s) as a function of temperature in the range 300^{o}C to 600^{o}C measured with an applied field of 10 kOe in the amorphous state for the nanocrystalline amorphous samples with composition $Fe_{72.5}Cr_1Nb_3Cu_1Si_{13.5}B_9$ are shown in Figure 4.8. The magnetization of the sample decreases gradually with increasing temperature since the thermal energy is acting on opposition to the magnetic coupling or exchange energy between neighboring atoms.

It is clearly observed from the curves of Figure 4.8 that the saturation magnetization of the sample decreases gradually. It is also noticed that magnetization at low temperature decreases slowly with the increase of temperature and falls faster the T_c. Therefore during the measurement of T_c of the heating rate should be adjusted in such a way so that no substantial relaxation and crystallization take place. From these curve T_c has been determined as the temperature corresponding to infixion point where the rate of change of magnetization with respect to temperature is maximum shown in Figure 4.9. As the temperature approaches to the T_c magnetization falls more rapidly near to zero as the thermal energy exceeds the magnetic ordering or the exchange energy.

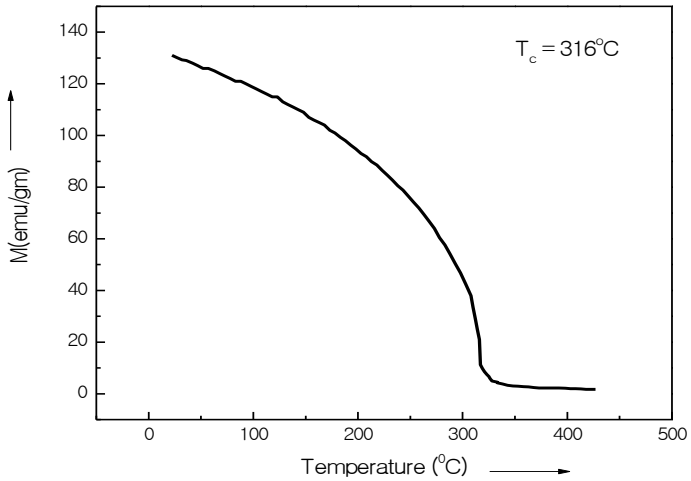

Figure 4.8 Temperature dependence of specific magnetization of amorphous nanocrystalline ribbons with composition $Fe_{72.5}Cr_1Nb_3Cu_1Si_{13.5}B_9$ alloys at constant applied field 10 kOe

Figure 4.9 shows the T_c determined in this method varies 100°C to 450°C for one percent Cr within an experimental ±2°C, since magnetization was recorded. The sharp fall of M_s at T_c indicates that the material is quite homogeneous for the point to view of amorphousity, the sharp fall of M_s are observed at 316°C for experimental sample shown in Figure 4.9.

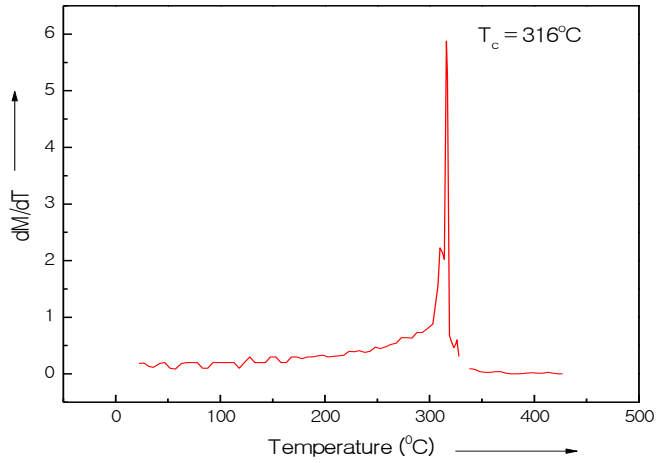

Figure 4.9 $\frac{dM}{dT}$ versus temperature curve of amorphous Nanocrystalline ribbon with composition $Fe_{72.5}Cr_1Nb_3Cu_1Si_{13.5}B_9$

The accurate determination of T_c of amorphous material is really difficult due to irreversible components of structural relaxation like long range internal stress, topological and chemical short range order. From the above measurements it has been elucidated that the thermos magnetic measurement is a powerful technique to analyze the crystallization behavior of amorphous ferromagnetic materials provided the crystallization products are ferromagnetic and the T_c of amorphous alloys lie below the crystallization temperature.

CONCLUSIONS

5.1 Conclusions

Nanocrystalline amorphous ribbon of FINEMET family with composition $Fe_{72.5}Cr_1Nb_3Cu_1Si_{13.5}B_9$ has been studied to find out the correlation between microstructural features and soft magnetic properties dependent on various stages of nanocrystallization during the isothermal annealing around the crystallization temperature of their amorphous precursors. These nanocrystalline alloy is as thin as 20-22μm in the amorphous state can be produced by melt spinning technique. This in turn has been aimed at furthering the understanding of crystallization of FINEMET alloys. The crystallization behavior of the sample was investigated by DTA and XRD experiments. The amorphous and annealed samples were examined by XRD to identify the microstructure of the sample. Magnetization measurement as a function of temperature and field were performed by VSM. The magnetic phase transition temperature i.e. Curie Temperature (T_c) was obtained from temperature dependence magnetization measurement. From the systematic investigation on the crystallization structural and magnetic properties the following conclusions can be obtained:

I. DTA experiments were performed for six different heating rates 10 to 60^{o}C/min. in steps of 10^{o}C/min. up to a temperature of 800^{o}C. DTA reveals the primary and secondary crystallization onset temperatures with the manifestation of two well obtained exothermic peaks corresponding to nanocrystalline α-Fe(Si) $\left(T_{x_1}\right)$ and Fe_2B $\left(T_{x_2}\right)$ phases respectively. The knowledge of the crystallization temperatures has been fruitfully utilized during the isothermal annealing of these amorphous ribbon for nanocrystallization, which ultimately controls the magnetic properties of FINEMET alloys. For heating rates 10^{o}C, 20^{o}C, 30^{o}C, 40^{o}C, 50^{o}C and 60^{o}C/min, the onset of $\left(T_{x_1}\right)$ were found 513^{o}C, 531^{o}C, 540^{o}C, 543^{o}C, 542^{o}C and 542^{o}C and that of the $\left(T_{x_2}\right)$ were found 692^{o}C, 707^{o}C, 713^{o}C, 717^{o}C, 722^{o}C and 712^{o}C respectively. The advantages realized are higher saturation induction and better thermal stability with soft magnetic properties at application temperature.

II. The temperature difference between two crystallization peaks ($T_{p2} - T_{p1}$) are found to exists around 168°C – 175°C. This peak separation temperature is important for the stability of α-Fe(Si) phase against detrimental Fe_2B phase while it is necessary for fabrication of higher quality inductors.

III. The activation energy values of the $\alpha - Fe(Si)$ and Fe_2B phases calculated using Kissinger's plots were 3.26 eV and 4.871 eV respectively.

IV. The amorphous stage of the as-cast ribbon has been confirmed by XRD. The evolution of primary phase on annealed samples has been confirmed as α-Fe(Si) and their sizes have been determined from the line broadening of fundamental peaks (110) from XRD pattern as affected by annealing of amorphous $Fe_{72.5}Cr_1Nb_3Cu_1Si_{13.5}B_9$ alloy annealed at temperature in the range of 450°C to 800°C for 30 minutes is $\alpha - Fe(Si)$ phases with arrange grain size 10 to 30nm. From XRD experiment, the crystallization onset temperature for the sample is around 500°C which coincides well with the value obtained DTA. XRD study reveals the boride phase at around 700°C for the sample which is also consistent with DTA result. The lattice parameter and Si content % shows an inverse relationship indicating that Si diffuses in the crystalline phase at the initial stage of crystallization at 550°C at which Si content % increased up to 650°C. Beyond 650°C, Si content % is found to decrease with increase in lattice parameter, that indicates diffusion of Si out of nanograins, indicating recrystallization i.e. formation of boride phase.

V. The saturation magnetization (M_s) value of sample at room temperature is 122.6emu/gm. The T_c of samples has been determined by temperature dependence saturation magnetization. The sharp fall of M_s at T_c indicates that the material is quite homogeneous for the point to view of amorphousity. The sharp fall of M_s is observed at 316°C. For technological uses of nanocrystalline materials at elevated temperature and for thermomagnetic stability it is important to 100K for composition that give higher values of T_c.

VI. The $Fe_{72.5}Cr_1Nb_3Cu_1Si_{13.5}B_9$ alloy has been synthesized by small addition of Cr by 1% in the original FINEMET composition. The change in properties as a result of addition of Cr found in our experiment includes:

   a) Achievement of soft magnetic nanograin form in the amorphous alloy is lower heat treatment than the original FINEMET.

b) Near value of T_c comparing to the original FINEMET sample indicates that the another improvement of thermo-magnetic stability due to lower concentration Cr addition.

5.2 Scope for Future Work

There is much scope for future research in controlling the magnetic characteristics by changing composition and heat treatment certain important parameter like temperature dependence of magnetization, anisotropy magnetostriction and Mössbauer effect can be study in detail for a better understanding of microstructure property relationship of Cr-based FINEMET type alloys. The playground of microstructural engineering of magnetic properties will undoubtedly progressed after new discoveries for further materials scientists and engineers.

REFERENCES

Chapter I

[1.1] Yoshizawa Y., Oguma S. and Yamauchi K.; "New Fe-based soft magnetic amorphous alloys composed of ultrafine grain structure"; J. Appl. Phys. 64 (10), 6044 - 6046, 1988.

[1.2] Vlasák G., Ŝvec P. and Duhaj P.; "Evolution of magnetostriction in $Fe_{73.5}Ni_xCu_1Nb_3Si_{13.5}$ B_9 (x = 0, 10, 20, 30, 40) alloy in the course of transformation;" J. Magn. Magn. Mat., 254, 225 - 227, 2003.

[1.3] Ohnuma M., H. Ping D., Abe T., Onodera H., Hono K. and Yoshizawa Y.; "Optimization of the microstructure and properties of co-substituted Fe-Si-B-Nb-Cu nanocrystalline soft magnetic alloys", J. Appl. Phys., Vol.93, No.11, 9186 - 9194, 2003.

[1.4] Herzer G.; "Grain Structure and Magnetism of Nano Crystalline Ferromagnetic"; IEEE Terns. Magn., 26, 1397 – 1402, 1990.

[1.5] Kulik T. and Hernando A; "Magnetic properties of two-phase nanocrystalline alloy determined by anisotropy and exchange interaction through amorphous matrix"; J. Magn. Magn. Mat., 138, 270 – 280, 1994.

[1.6] Mondal S. P., Kazi Hanium Maria, Sikder S. S., Shamima Choudhury, Saha D. K. and Hakim M. A.; "Influence of Annealing Condition on Nanocrystalline and Ultra - Soft Magnetic properties of $Fe_{75.5}Cu_1Nb_1Si_{13.5}B_9$ alloy"; J. Mater Sci. Technol., 28(1), 21 - 26, 2012.

[1.7] Saroaut Noor, Sikder S. S., Saha D. K. and Hakim M. A.; "Time and Temperature dependence of Nanocrystalline and initial permeability of Finemet alloy"; Nuclear Science and application, 15, 1, 9 - 13, 2006.

[1.8] Herzer G.; "Nanocrystalline soft magnetic alloys", Chapter 3 in Hand Book of materials; Vol.10 ed. K.H. J. Buchow, Elsevier Pub. Co. P.417, 1997.

[1.9] Hakim M. A.; "Magnetic softening of nanocrystalline FeCuNbSiB alloys on annealing"; J. Bangladesh Electronic Socity, 4, 40 – 45, 2004.

[1.10] Kazi Hanium Maria, Mondal S. P., Shamima Choudhury, Sikder S. S., Hakim M. A. and Saha D. K.; "Effect of Annealing Temperature on the Soft Magnetic Properties of $Fe_{75.5}Cu_1Nb_1Si_{13.5}B_9$ Amorphous Alloys", Journal of Emerging Trends Sciences (JETEAS), 2(1). 102 – 108, 2011.

[1.11] Hakim M. A., Sikder S. S., Md. Sultan Mahmud and S. Manjura Hoque; "Dilution of magnetic moment of Fe by Cr for $Fe_{73.5-x}Cr_xNb_3Cu_1Si_{13.5}B_9$ and field cooled and zero field cooled behavior for higher Cr-Content"; Journal of Korean physical Society (JKPS), 52, 5, 2008.

[1.12] Alben R., Becker J. J. and Chi M. C.; "Random anisotropy in amorphous ferromagnets", J. Appl. Phys., 49, 19 - 53, 1978.

[1.13] G. Herzer; In: Buschow KHJ Editor, "Hand book of magnetic materials"; Amsterdam: Elsevier Science, 10, 415, 1997

[1.14] N. Murillo, J. Gonzalez, J. M. Blanco, J. M. Gonzalez; J. Appl. Phys. ,79, 5465, 1996

[1.15] Le Minh, Bach Thanh Cong, Tran Quoc and Nguyen Chau; Proceding of the 2nd International Workshop on Materials Science (IWOMS'95) Hanoi, Oct. 1995

[1.16] E. Estevez Rams, J. Fidler, M. Dahlgren, R. Grossinger, M. Knobel, P. Tiberto, P. Alia and F. Vinal; J. Phys. D; Appl. Phys. **29** 848-854, 1996

[1.17] Saroat Noor, M. Phil Thesis, Department of Physics, KUET, Khulna, March-2005

[1.18] Saroat Noor, S. S. Sikder, D. K. Saha and M. A. Hakim; "Time and Temperature Dependence of Nanocrystallization and initial Permeability of FINEMET alloy"; Nuclear Science and Applications, 15, 1, 9 - 13, 2006

[1.19] Y. Yoshizawa and K. Yamauchi; "Fe-based soft magnetic alloys composed of ultrafine grain structure"; Materials Transaction. JIM. 31, 4, 307 - 314, 1990

[1.20] Judit Kopniczky; "Nanostructures studied by atomic force microscopy"; Ph.D. Thesis, Uppsala University, Sweden, 2003

[1.21] T. H. Noh, M. B. Lee, H. J. Kim, I. K. Kang "Relationship between crystallization process and magnetic properties of Fe-(Cu-Nb)-Si-B amorphous alloys", J. Appl. Phys 67, 5568, 1990

[1.22] N. Kataoka, T. Matsunaga, A. Inoue, T. Masumoto; "Soft magnetic properties of b.c.c Fe-Au-X-Si-B (X=early transition metal) alloys with fine grain structure"; Mater. Trans. JIM. 30, 947-950, 1989

[1.23] M. Müller and N. Matern; "The influence of refractory element additions on the magnetic properties and on the crystallization behavior of nanocrystalline soft magnetic Fe-B-Si-Cu alloys"; J. Magn. Magn. Mater. 136, 79, 1994

[1.24] P. K. Roy; M. Phil Thesis, Department of Physics, KUET, Khulna, May - 2007

[1.25] A. Inoue, K. Kobayashi, J. Kanerhira and T. Masumoto; "Mechanical properties and thermal stability of (Fe-Co-Ni)-M-B (M = IV, V and VI group transition metals) amorphous alloys with low Boron concentration"; Sci. Rep. Res. Inst. Tohoku Univ. **A** 29, 331 - 342, 1981

[1.26] K. Suzuki, A. Makino, N. Kataoka, A. Inoue, and T. Masumoto; "Soft magnetic properties of nanocrystalline b.c.c. Fe-Zr-B and Fe-M-B-Cu (M= transition metals) alloys with high saturation magnetization"; J. Appl. Phys., 70(10), 6232, 1991

[1.27] K. Suzuki, A. Makino, A. Inoue, and T. Masumoto; "Low core losses of nanocrystalline Fe-M-B (M = Zr, Hf or Nb) alloys"; J. Appl. Phys., 74, 3316, 1993

[1.28] G. Herzer; "Grain Size dependence of Coercivity and Permeability in nanocrystalline ferromagnets" IEEE Trans. Mag. 26(5), 1397-1402, 1990

[1.29] A. Hakim, S. Manjura Haque; "Effect of structural parameters on soft magnetic properties of two phase nanocrystalline alloy of $Fe_{73.5}Ta_3Cu_1Si_{13.5}B_9$" J. Magn. Magn. Mater, 284, 395-402, 2004

[1.30] S. Manjura Haque, A. Hakim; "Ultra-soft magnetic properties of devitrified $Fe_{75.5}$ $Cu_{0.6}Nb_{2.4}Si_{13}B_{8.5}$" J. Materials Chemistry and Physics, **101,** 112-117, 2007

[1.31] V. Franco, C. F. Conde, A. Conde, L. F. Kiss; "Super paramagnetic behavior in a $Fe_{76}Nb_3Cu_1Si_{10.5}B_{9.5}$ alloy" J. Magn. Mater. 215-216, 400-403, 2000

[1.32] M. A. Hakim; "Magnetic softening of nanocrystalline Fe-Cu-Nb-Si-B alloys on annealing"; J. Bangladesh Electronic Society; Vol. 4 pp. 40-45, 2004

[1.33] A. Slawska –Wanicwska, M. Gutowski, H. Lachowicz, T. Kulix, M. Matiya; Phys. Rev. B 46, 14 594, 1992

[1.34] H. K. Lachowicz, A. Slawska –Wanicwska; J. Magn. Magn. Mat., 133, 238, 1994

[1.35] Md. Sultan Mahmud, S. S. Sikder and M. A. Hakim; "Crystallization behavior and Initial Permeability of Fe (Cr) Cu Nb Si B Nanocrystalline alloys"; Journal of Science & Arts, Issue 1, 1, 33 - 41, 2004

[1.36] N. Chau, P. Q. Thanh, N. Q. Hoa and N. D. The, "The existence of giant magnetocaloric effect and laminar structure in $Fe_{73.5-x}Cr_xNb_3Cu_1Si_{13.5}B_9$"; J. Magn. Mater. **304,** 36-40, 2006

[1.37] N. Chau, P. T. Hue, N. Q. Hoa, H. D. Anh, N. H. Luong, M. A. Asgar, S. S. Sikder, Md. Sultan Mahmud; "An existence of Laminar Structure in nanocrystalline ribbon in finemet with partial substitution of Fe by Cr". Proceedings of the seventh Vietnamese – German Seminar on Physics and Engineering, Halong City, March 28 to April 5, 2004

[1.38] D. K. Saha and M. A. Hakim; "Crystallization behavior of $Fe_{73.5}Au_1Nb_3Si_{13.5}B_9$ Amorphous Nanocrystalline soft magnetic alloy"; Bangladesh Academy of Science, 30, 2, 177 - 187, 2006

[1.39] M. A. Hakim,S. S. Sikder, Md. Sultan Mahmud and S. Manjura Hoque; "Dilution of magnetic moment of Fe by Cr for $Fe_{73.5-x}Cr_xNb_3Cu_1Si_{13.5}B_9$ and field called and zero field cooled behavior for higher Cr-content"; Journal of Korean Physical Society (JKPS), 52, 5, 2008

[1.40] Md. Sultan Mahmud; PhD thesis, Department of Physics, KUET, Khulna, April, 2008

Chapter II

[2.1] Yoshizawa Y., Oguma S and Yamauchi K; "New Fe-based soft magnetic amorphous alloys composed of ultrafine grain structure", J. Appl. Phys. 64(10), 6044 – 6046, 1988.

[2.2] Herger G.; "Grain size dependence of coercivity and permeability in nanocrystalline ferromagnets", IEEE Trans. Magn. 26(5), 1397 – 1402, 1990.

[2.3] P. Duwez; J. Am Inst. Metal Eng. 191: 765, 1951

[2.4] P. Duwez, R. H. Willens and W. Klement; J. Appl. Phys. 31, 1136, 1960

[2.5] P. Duwez; Trans. Am SOC Met. 60: 607, 1967

[2.6] P. Duwez; Ann Rev. Mat. Sci. 6: 83, 1967

[2.7] S. Mader; Nowick As.; Appl. Phys. Lett. 7: 57, 1965

[2.8] C. C. Tsuei, P. Duwez; J. Appl. Phys. 37: 435, 1960

[2.9] M. A. Mc Henry, M. A. Willard and D. E. Laughlin; "Amorphous and nanocrystalline materials for applications as soft magnets"; Prog. Mat. Sci. 44 291- 433, 1999

[2.10] T. Mizoguchi; IBM Research report, RC 6045, 1976

[2.11] R. Alben, J. I. Budnic and G. S. Gargil; a_{111} Metalicglasess, "American SOC. for metals"; 304, 1978

[2.12] Y. Yoshizawa, S. Ogma and K. Yamauchi; "New Fe-Based Soft Magnetic Alloys Composed of Ultra-fine Grains Structure"; J. Appl. Phys. 64, 6044, 1988

[2.13] Y. Yoshizawa and K. Yamachi; "Magnetic Properties of Fe-Cu-M-Si-B (M = Cr, V, Mo, Nb, Ta, W) alloy"; Mater. Sci. Eng. A (b). 133, 176, 1991

[2.14] Y. Yoshizawa and K. Yamachi; "Fe-based soft magnetic alloys composed of ultra-fine grains structure"; Mater.Trans. JIM. (a) 31, 307, 1990

[2.15] G. Herzer, H. Warlimont; Nanostructured materials, 1, 263-268, 1992

[2.16] K. Hono and T. Sakurai; "Atom Probe studies of nanostructured alloys"; Appl. Surf. Sci. 87/88,166, 1995

[2.17] K. Hono, K. Higara, Q. Wang, A. Inoue and T.Sakurai; "The microstructure evolution of a $Fe_{73.5}$ Nb_3 Cu_1 $Si_{13.5}$ B_9 nanocrystalline Soft Magnetic material"; Acta. Metall. Mater. 40(9) 2137-2147, 1992

[2.18] G. Herzer; "Nanocrystalline Soft Magnetic Alloys"; Hand Book of Materials, K. H. J. Buchow (ed), 10, 415-462, 1997

[2.19] G. Herzer; In: Proc of Int. Symp. On 3ab Transition-Semi Metal Thin Films. Magnetism and Processing (Japan SOC for the promotion of Science, Committee, Sendia, Japan) **131** 130, 1991

[2.20] H. warliment; Mater. Sci. Eng. 99, 1988

[2.21] A. Makino, A. Inoue, T. Masumoto; Mat. Trans. JIM **36,** 924, 1995

[2.22] Jones H., Rep. Prog. Phys., **36,** 1425, 1973

[2.23] Turnbull D., J. dc physique, **35,** C4 - 1, 1974

[2.24] Takayama S.; "Amorphous structure and their formation and stability"; J. Materials Sci. 11(1), 164 - 185, 1976

[2.25] Irvine J. T. S., Amano E., Huanosta A., Valenzuela R. and West A. R.; "Solid State should peak at T_c"; Ionic 40/41, 220, 1990

[2.26] Cohen M. H. and Turnbull D.; "Composition Requirements for Glass Formation in Metallic and Ionic Systems"; Nature 189 131-132, 1961

[2.27] Gargil G., III; J. Appl. Phys, 41, 2248, 1970

[2.28] Chen H. S.; Acta. Mat. 22, 1505, 1974

[2.29] Nageland S. R. and Taue J.; "Nearly- free- electron Approach to the theory of Metallic Glass Alloys"; Phys. Rev. Lett., 35, 380, 1975

[2.30] Berkowitz A. E., Walter J. L.and Wall K. F.; " Magnetic Properties of amorphous particles produced by Spark Erosion"; Phys. Rev. Lett. 46, 1484, 1981

[2.31] Murray P. and White J.; "Kinetics of the thermal dehydration of clays"; Trans. Brit. Ceram. SOC. 48, 187-206, 1949

[2.32] Murray P. and White J.; "Kinetics of the thermal decomposition of clay 2, Isothermal decomposition of clay materials"; Trans. Brit. Ceram. SOC. 54, 151-187, 1955

[2.33] Murray P. and White J.; "Kinetics of the thermal decomposition of clay 4, Interpretation of the differential thermal analysis of clays", Trans. Brit. Ceram. Soc. 54, 204-237, 1955

[2.34] Sewel E. C.; "The consequences for differential thermal analysis of assuming a reaction to be first order"; Clay Minerals Bul. 2, 233-241, 1955

[2.35] Kissinger H. E.; "Reaction Kinetics in Differential Thermal Analysis"; Anal. Chem. 29(11) 1702-1706, 1957

[2.36] Boswell F. G.; "On the calculation of activation energies using a modified Kissinger method"; J. Therm. Anal. 18(2) 353-358, 1980

[2.37] Cullity B. D.; "Elements of X-Ray diffraction"; Reading, M.A. Addisonwesley, 1978

[2.38] Bozorth R.; "Ferromagnetism", D. Van Nostrand, Princeton N. J. 76, 1951

[2.39] Bozorth; "Ferromagnetism" , D. Van Nordtrand Company, Inc. Priceton, NJ, p.64, 1964.

Chapter III

[3.1] D. Turnbull; Contemp. Phy. 10, 473, 1969

[3.2] P. Duwez , R. H. Willens and W. kelment Jr.; J Appl. phy. 31, 1136, 1960

[3.3] JMD. Coey and H. Sun; J. Magn. Mater. **87** 1251, 1991

[3.4] K. Schnitzke, L. Schultz, J. Wecker and M. Katter; Appl. Phys. Lett., **57** 2853, 1990

[3.5] H. Le Chatelier; Bull SOC. France Mineral, 10, 204, 1987

[3.6] W. B. Pearson; "A Hand book of Lattice spacing and Structures of Metals and Alloys" (Oxford Pergamon), 1958

[3.7] M. A. Mazid and M. A. Chowdhury; "Design and Construction of Forner type Vibrating Sample Magnetometer"; AECD/MMD/1 (Bangladesh). June, 1986

[3.8] Simon Foner; "Versatile and Sensitive Vibrating Sample Magnetometer"; Rev. Sci. Instr. 30, 160, 1959

Chapter IV

[4.1] M. E. Mc Henry, M. A. Willard and D. E. Laughlin; "Amorphous and nanocrystalline materials for applications as soft magnets." Prog. Mat. Sci. 44, 29-433, 1999

[4.2] S. Manjura Hoque, M. A. Hakim, N. Chau; "Ultra soft magnetic properties devitrified $Fe_{75.5}Nb_{2.4}Cu_{0.6}Si_{13}B_{8.5}$ alloy" Mat. Chem. Phys. 101, 112-117, 2007

[4.3] D. K. Saha and M. A. Hakim; Journal of Bangladesh Academy of Sciences; 30, 2, 177-187, 2006

[4.4] W. G. Clements and B. Cantor; in Rapidly quenched metal, Section-1, (eds. N. J. Graut and B. C. Giessen) (MIT Press Cambridge, Mass) P-267, 1976

[4.5] F. E. Luborsky; Materials Sci. Engg. - 28, P-139, 1977

[4.6] Chen C.L and Hasagawa R.S.; "Mössbaur Study of glassy alloy $(Fe\text{-}Mo)_{80}B_{20}$, J Appl. Phys. 49(3), 1721, 1978.

[4.7] S. Noor., "Effects of two-step annealing on complex permeability of Fe-Nb-Cu-Si-B nanocrystalline soft magnetic materials" M. Phil Thesis, , KUET, P 70-72, March 2005

[4.8] Noor S.; "Effects of two-step annealing on complete permeability of Fe-Nb-Cu-Si-B Nanocrystalline soft magnetic materials", M. Phill Thesis, KUET, P-70-72, March 2005.

[4.9] B. D. Cullity; "Elements of X-ray Diffraction"; Adison-Wisley Publishing Company Inc., London, England, 262, 1959

[4.10] Bozorth, "Ferromagnetism", D.Van Norstrand Company, Inc., Princeton, NJ, 64, 1964

[4.11] W. B. Pearson; "A Hand book of Lattice spacing and Structures of Metals and Alloys" (Oxford Pergamon), 1958

[4.12] Franco,V., Conde C.F., Conde A., "Changes in magnetic anisotropy distribution during structural evolution of $Fe_{76}Si_{10.5}B_{9.5}Cu_1Nb_3$" J. Mang. Mang. Mat. 185, 353 – 359, 1998

[4.13] Kneller, E. F., and Luborsky, F. E., "Particle Size Dependence of Coercivity and Remanence of Single-Domain Particle", J. Appl. Phys. 34, 656, 1963

[4.14] Cullity, B. D., "Elements of X-Ray Diffraction", Adison-Wisley publishing company Inc., London, England, 262, 1959

[4.15] M. A. Mazid and M. A. Chowdhury; "Design and Construction of Forner type Vibrating Sample Magnetometer"; AECD/MMD/1(Bangladesh), June, 1986

Conference Paper

1. **M. T. Shihab**, S. S. Sikder & A. Gafur "Study the Crystallization Phase and Magnetic Properties of Nanocrystalline $Fe_{72.5}Cr_1Nb_3Cu_1Si_{13.5}B_9$ Alloy" Interational Conference on Engineering Materials and Metallurgical Engineering (ICEMME), held on 22-24 December 2016, Pilot Plant and Process Development Centre (PP & PDC) Bangladesh Council of Science and Industrial Research (BCSIR), Dhanmondi, Dhaka, Bangladesh.